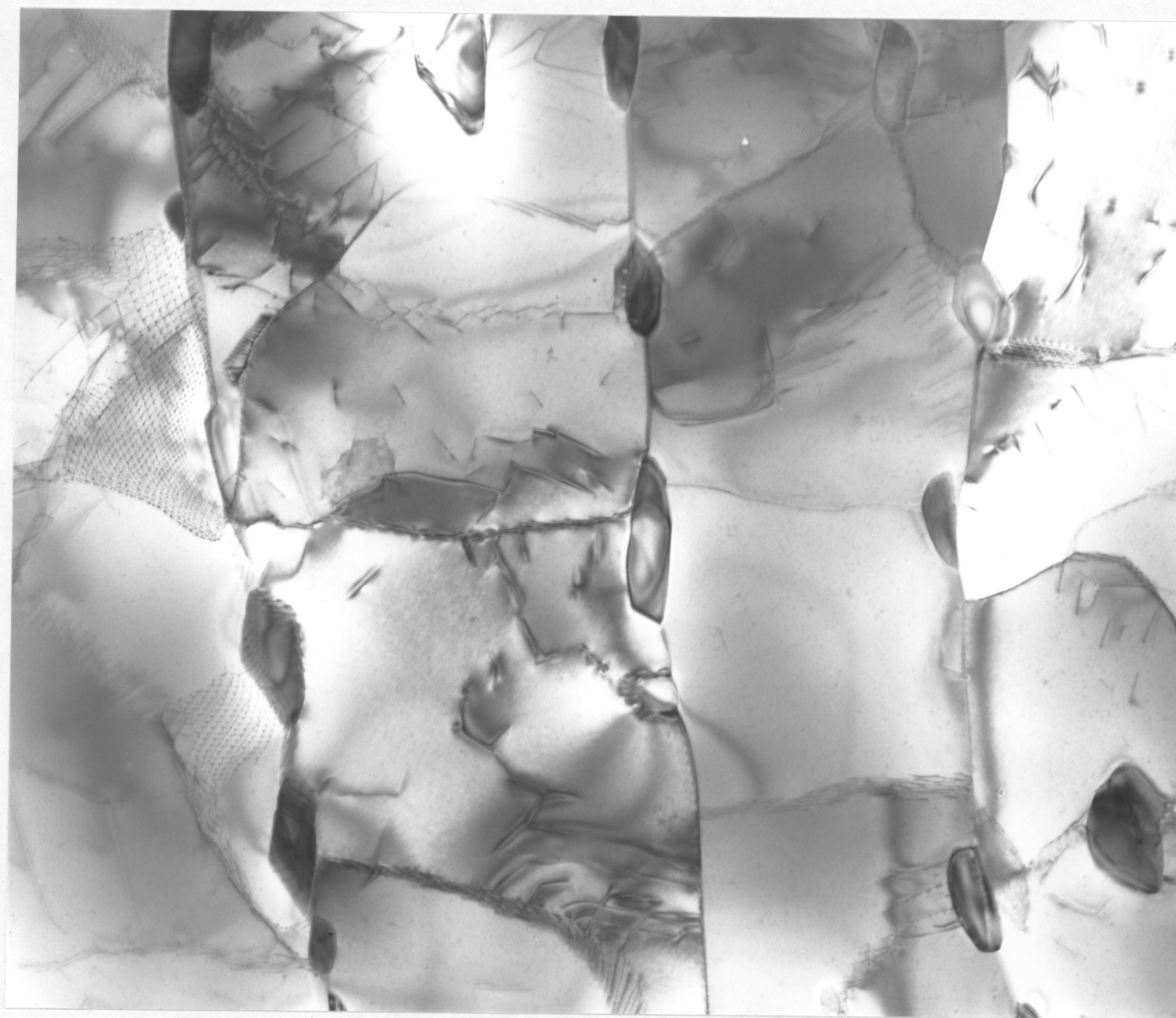Table VII.1 - Microanalytical data (wt.%, error ≈ ± 0.20) for the γ and α during reaustenitisation from starting microstructure α_b + γ.

Temp.(°C)	Time(hr)	MN γ	Mn α	Si γ	Si α
720	2	4.11	2.37	1.58	2.15
765	2	3.91	2.42	1.85	2.31
800	2	3.70	2.37	1.58	2.04
835	2	3.21	3.18	2.09	2.25
835	6.5	3.22	3.20	1.86	2.08

Figure VII.17 - 10 mins @ 950°C → 2 hrs @ 350°C → 42.7 hrs @ 600°C.

181

Figure VII.18 - Electron micrograph showing that the cementite particles are located at the gain boundaries of extensively recovered ferrite. Mesh-like subgrain boundaries are displayed in the left side of the micrograph. (10 mins @ 950°C → 2 hrs @ 350°C → 14 days @ 680°C).
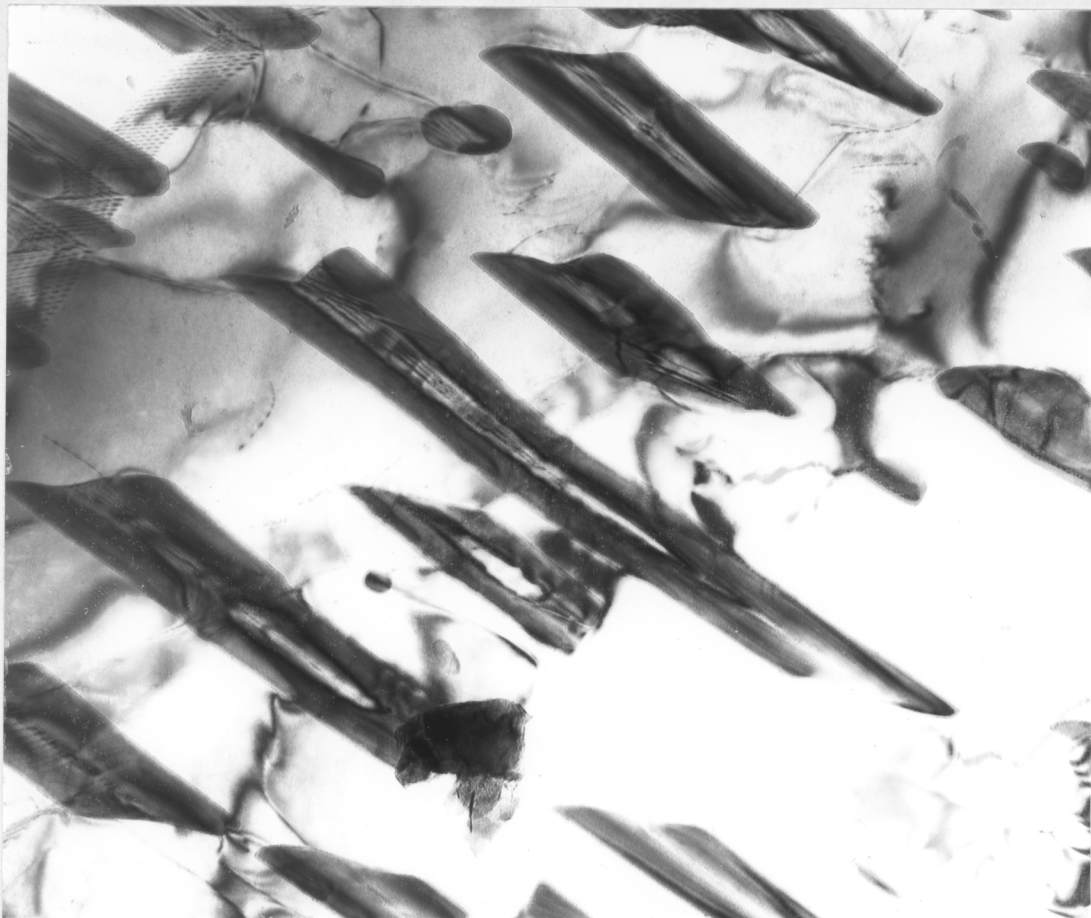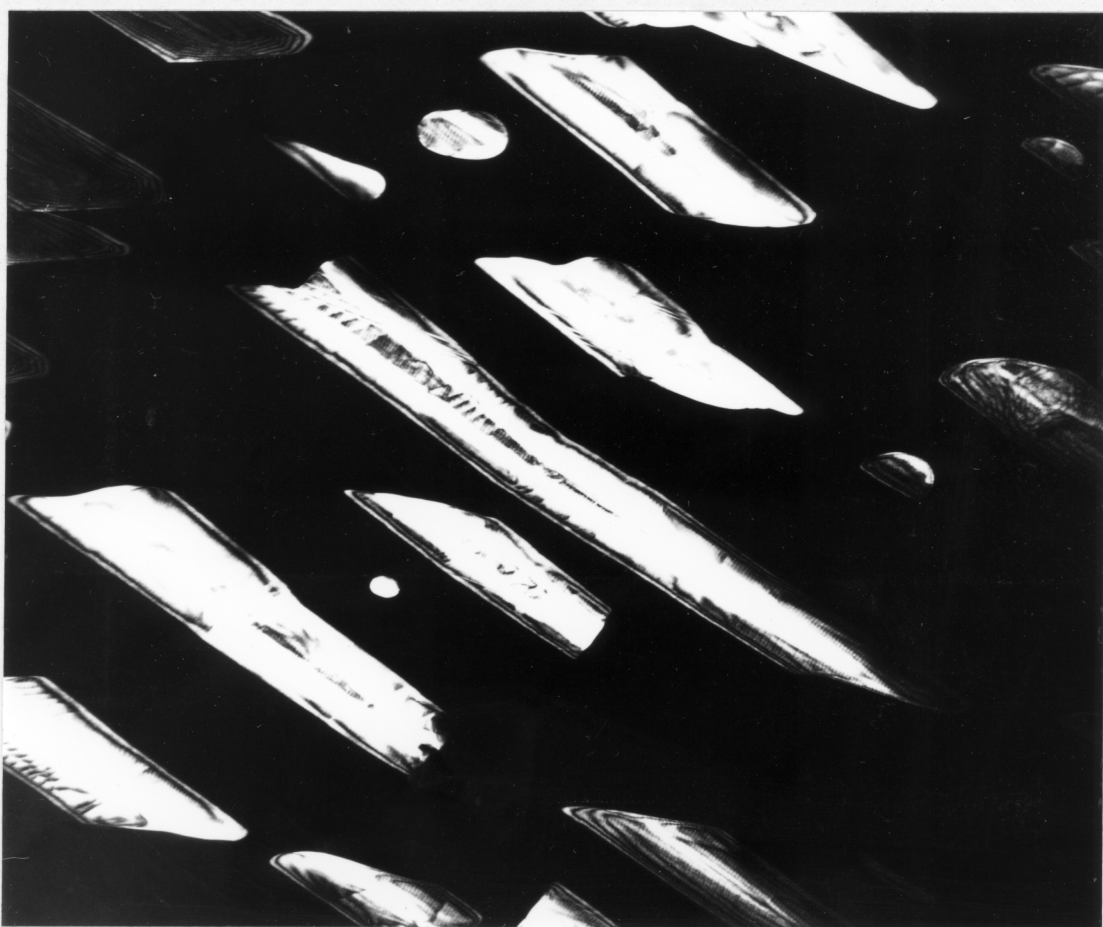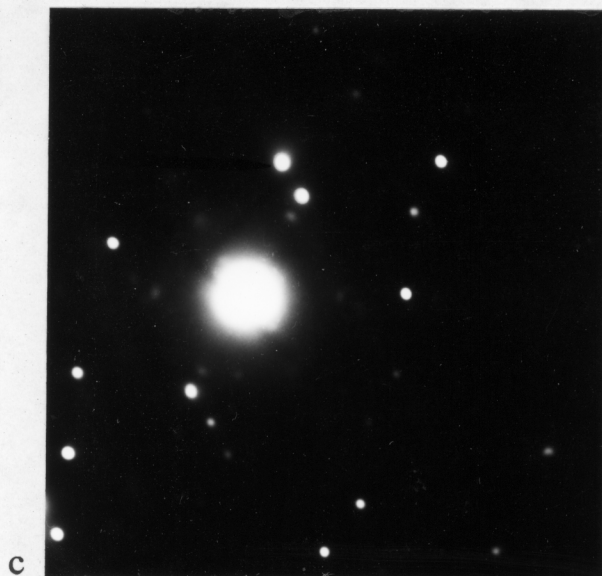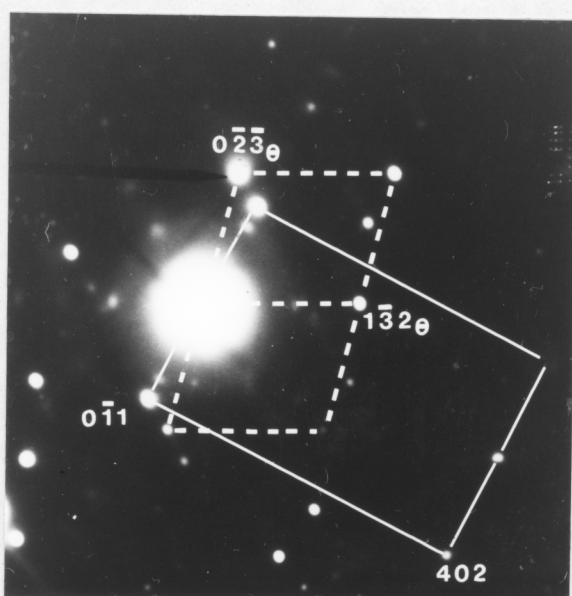
Figure VII.19a

Figure VII.19b

0·5 μm

c

d

Figure VII.19:
10 mins @ 950°C → 2 hrs @ 350°C → 30 mins @ 600°C → 25 mins @ 715°C.
(a) Bright field image.
(b) Cementite dark field image using $(0\bar{2}\bar{3})_\theta$ reflection.
(c) Corresponding diffraction pattern.
(d) Interpretation of (c).

184

a

0·5μm

b

c

Figure VII.20:
10 mins @ 950˚C → 2 hrs @ 350˚C → 30 mins @ 600˚C → 25 mins @ 715˚.
(a) Bright field image.
(b) Corresponding diffraction pattern.
(c) Interpretation of (b).

185

Figure VII.21a

Figure VII.21b
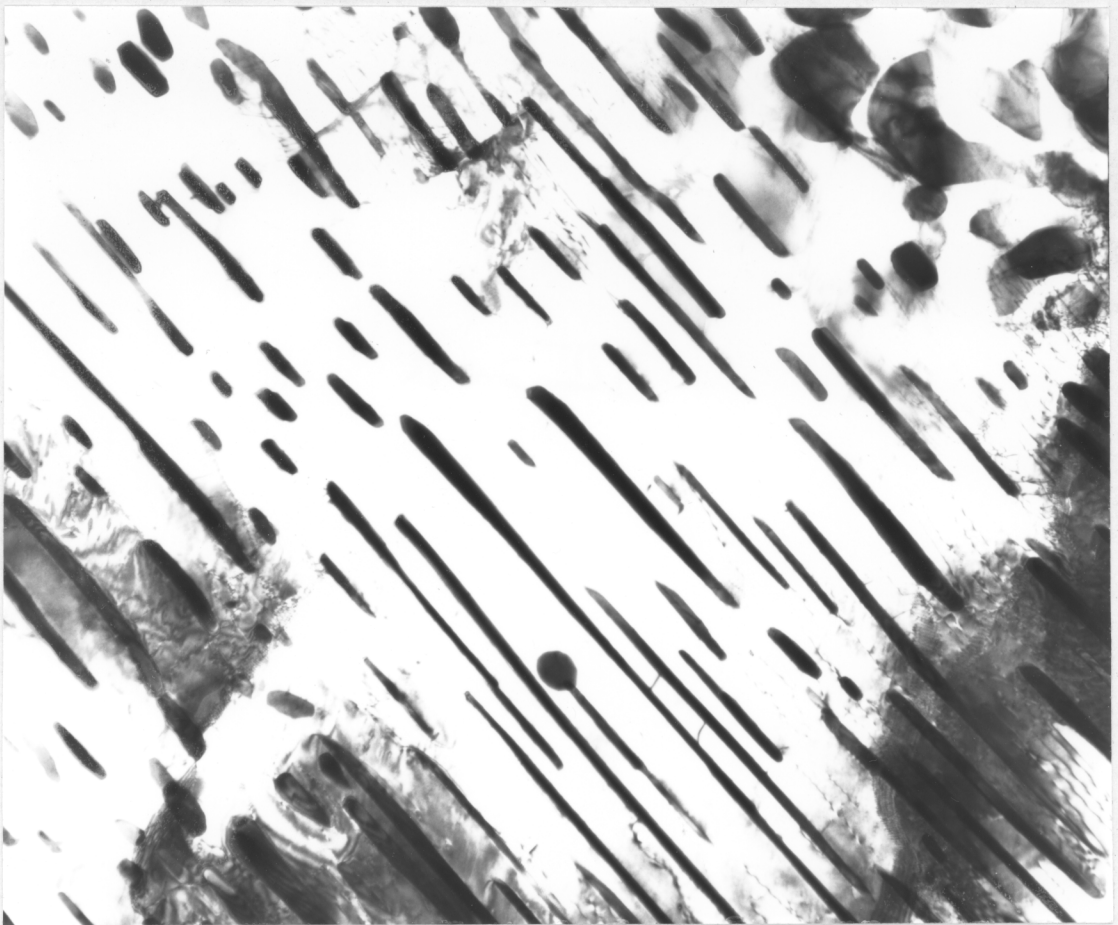
0·5 μm

Figure VII.21c

Figure VII.21d

Figure VII.21:
10 mins @ 950°C → 2 hrs @ 350°C → 30 mins @ 600°C → 25 mins @ 715°C.
(a) Bright field image.
(b) Cementite dark field image using $(210)_\theta$ reflection.
(c) Corresponding diffraction pattern.
(d) Interpretation of (c).

187

Figure VII.22a

Figure VII.22b

1·0 μm

Figure VII.22c

Figure VII.22d

Figure VI.22
10 mins @ 950°C → 2 hrs @ 350°C → 30 mins@ 600°C → 25 mins @ 715°C.
(a) Bright field image.
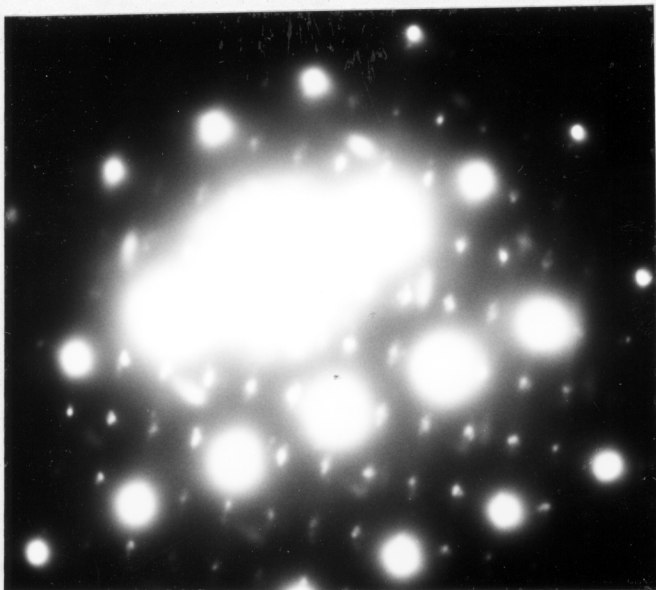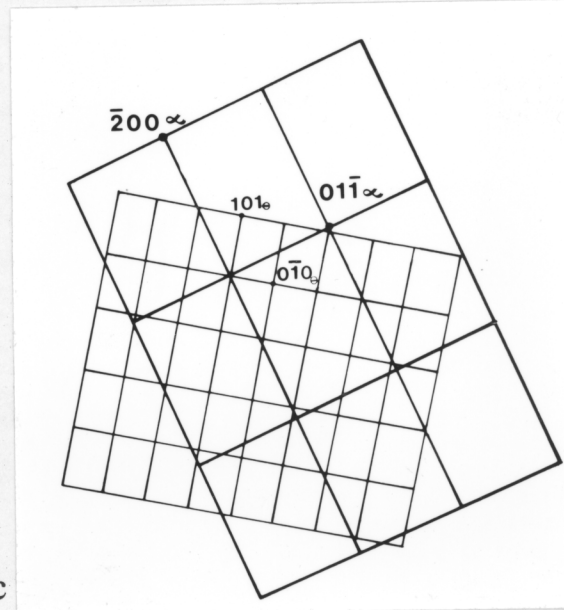(b) Cementite dark field images using $(0\bar{2}\bar{1})_\theta$ reflection.
(c) Corresponding diffraction pattern.
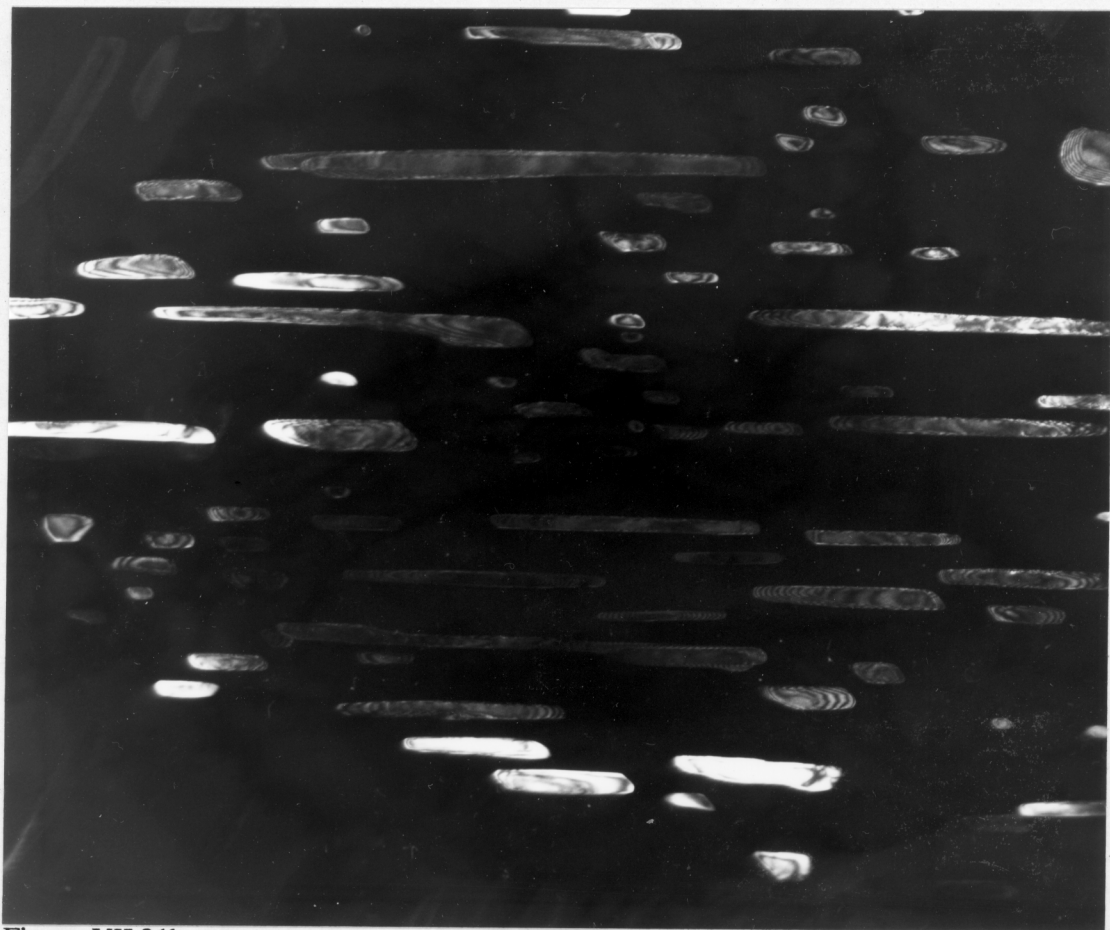(d) Interpretation of (c).

189

Figure VII.23a

Figure VII.23b

1·0 μm

Figure VII.23c
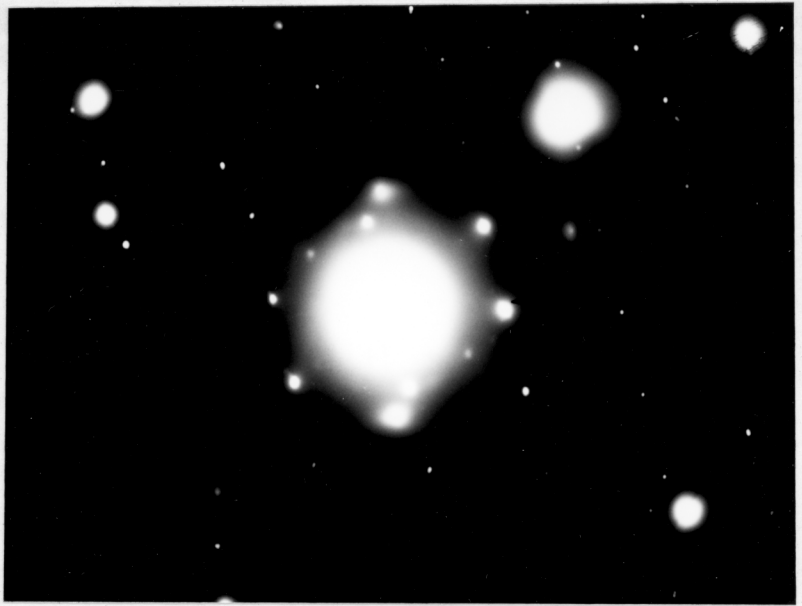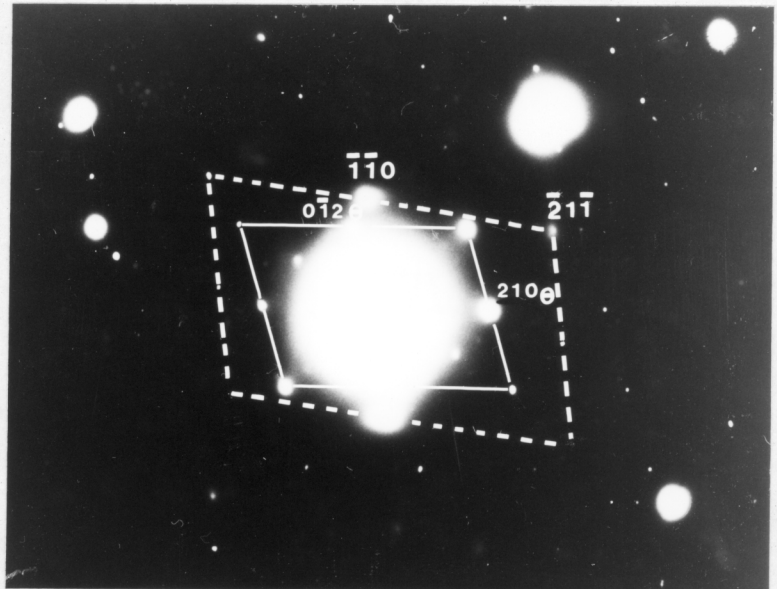

Figure VII.23d

Figure VII.23
10 mins @ 950°C → 2 hrs @ 350°C → 30 mins @ 600°C 25 mins @ 715°C.
(a) Bright field image.
(b) Cementite dark field image using $(0\bar{2}1)_\theta$ reflection.
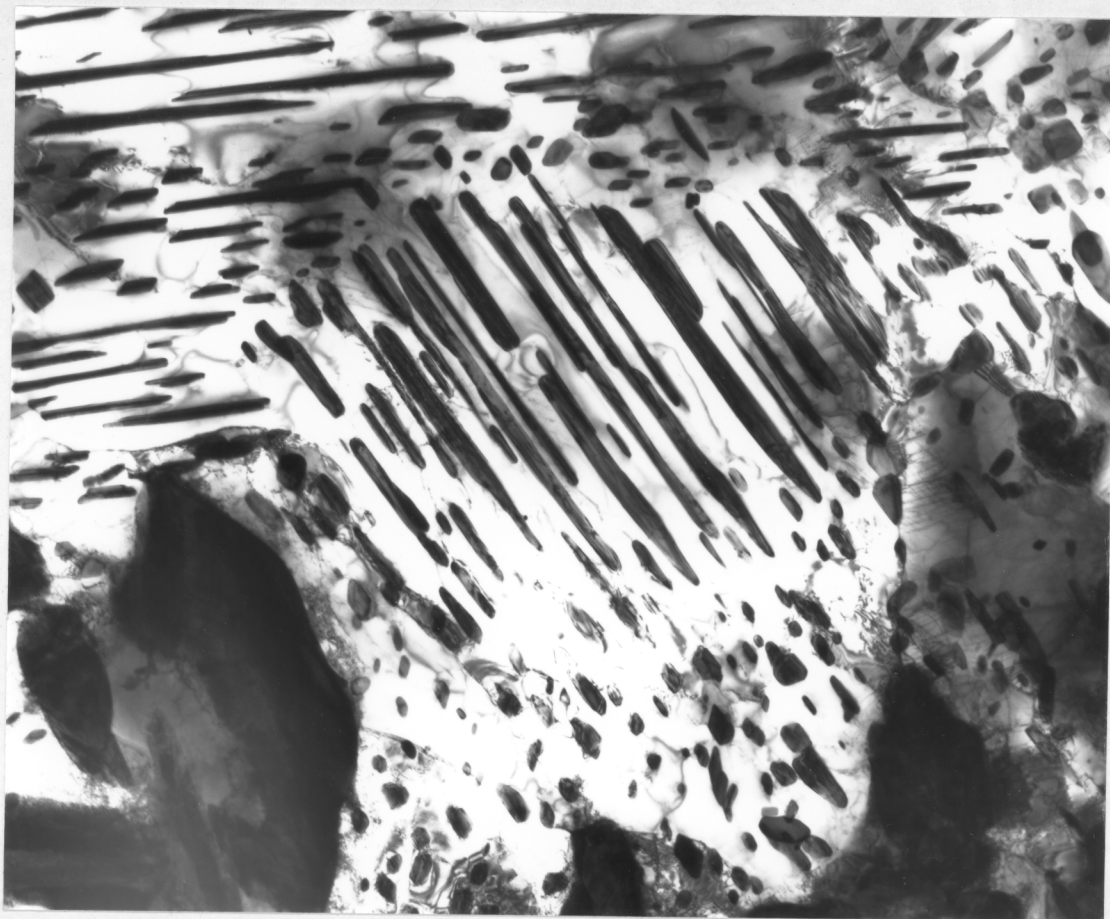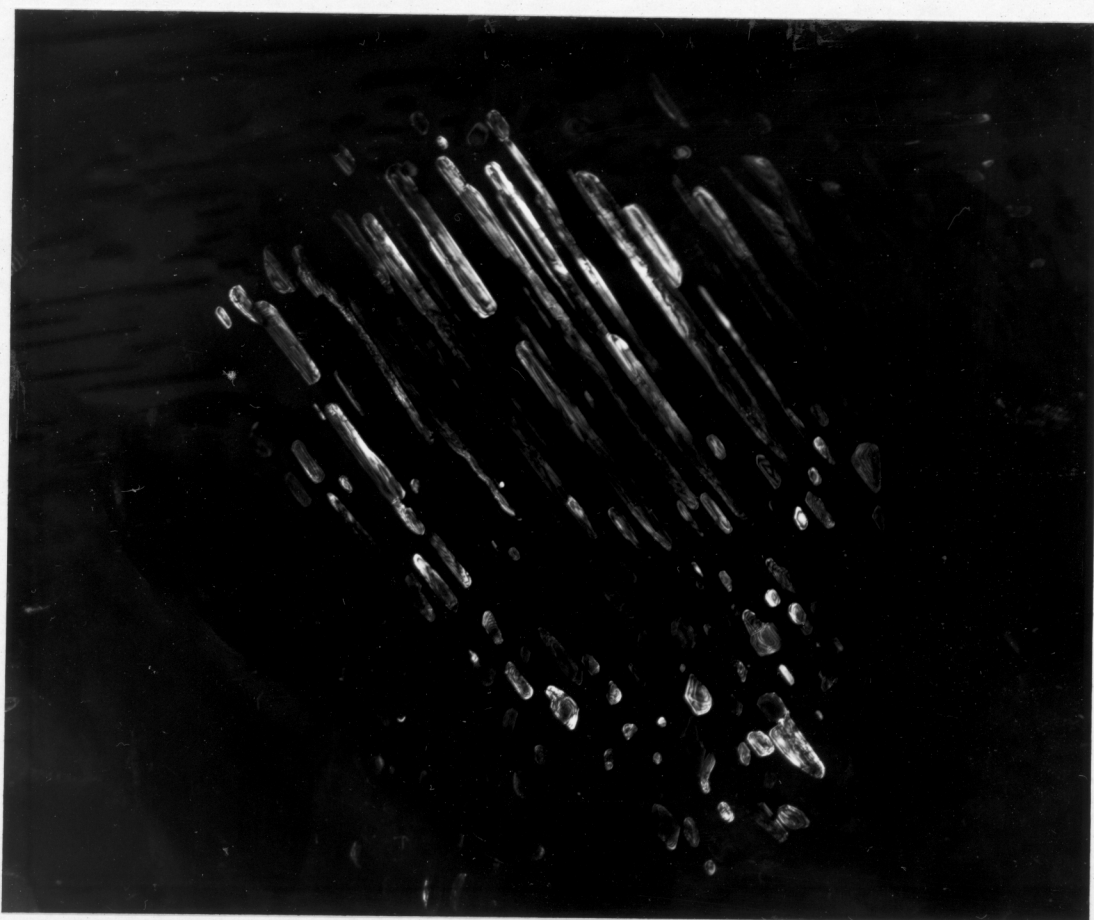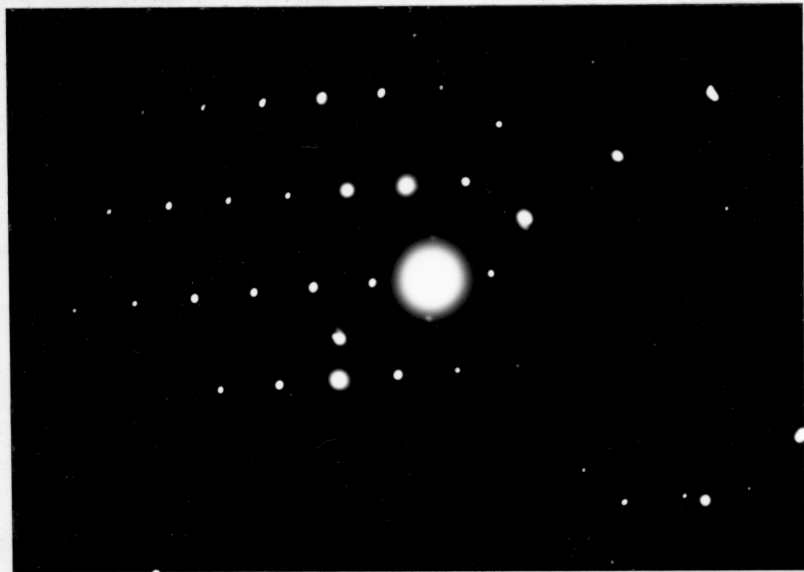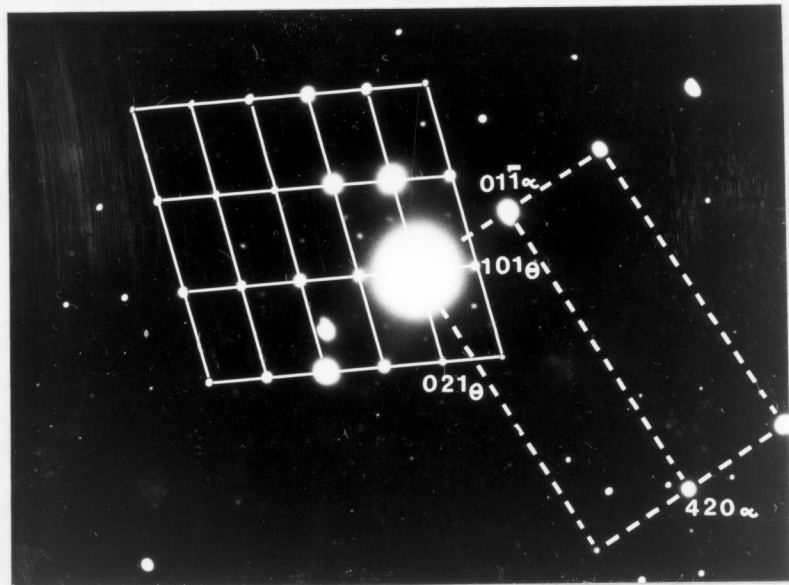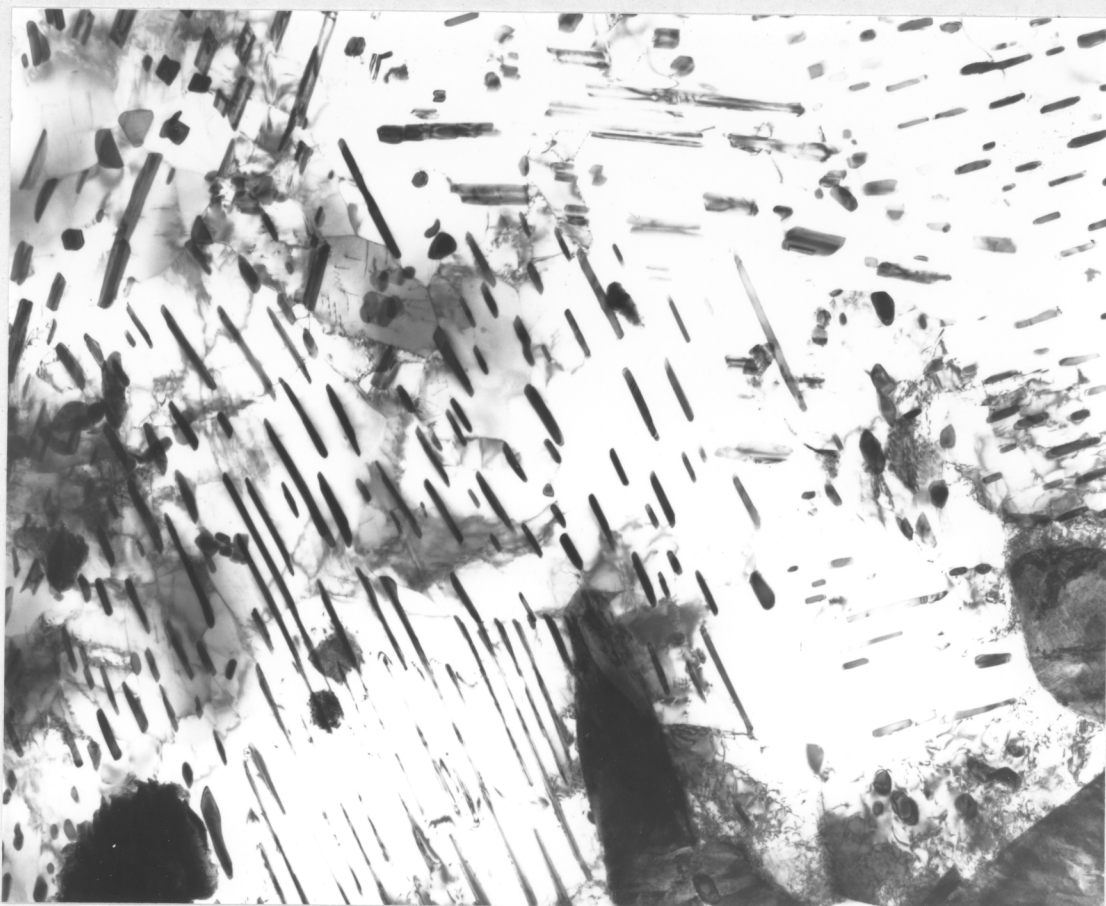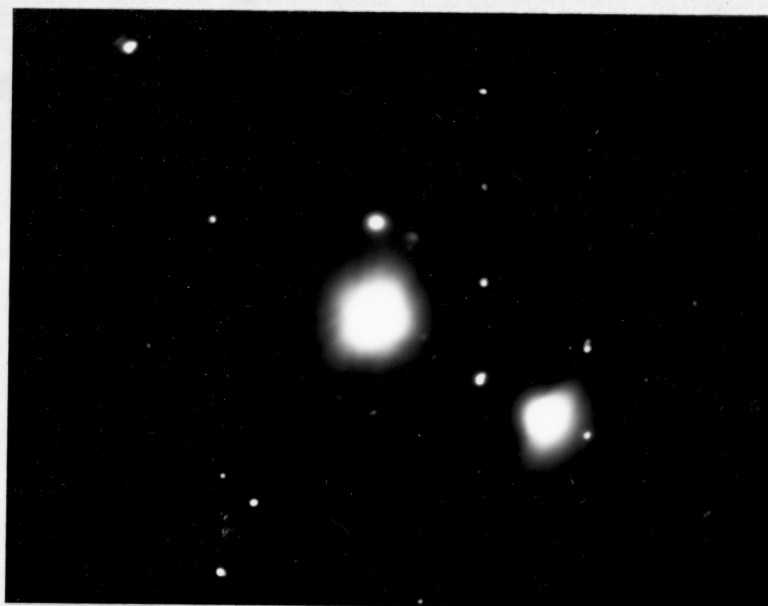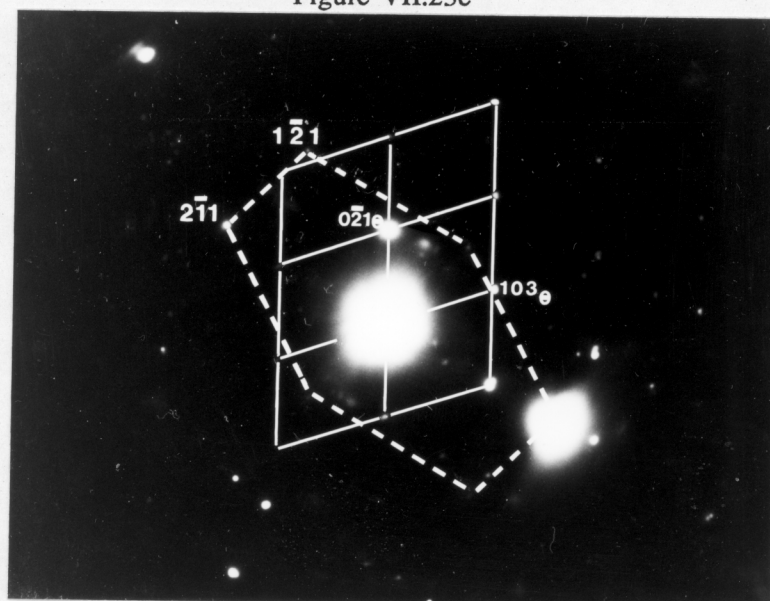(c) Corresponding diffraction pattern.
(d) Interpretation of (c).

191

Chapter Eight

The Microstructure of Heat Affected Zone

8.1 Introduction

During welding, microstructural changes occur within the heat affected zone (HAZ) of the base plate surrounding the molten weld-bead. Grain growth and the formation of martensite in this region are serious problems as far as mechanical properties are concerned. The larger austenite grain size displaces the C.C.T. curve to longer reaction times producing more Widmanstätten ferrite, or increasing the possibility of martensitic or bainitic transformation products on cooling. Although some work has been done [141-146] on the study of microstructure in HAZ, a model for directly predicting the microstructure has not yet been developed. At this stage, it is important to rationalise quantitatively the kinetics of austenite transformation, which depend on its grain size and chemical composition.

In this work, a low alloy steel has been investigated, and its composition is Fe-0.17C-0.33Si-1.42Mn (wt%). The microstructure of its heat affected zone has been examined and the kinetics of austenite transformation for different grain sizes also studied experimentally.

8.2 The Microstructure of the Heat Affected Zone in a Low Alloy Steel

The microstructure of the heat affected zone studied was taken from the parent plate of a high-strength weld. The plate thickness was 20mm and the arc energy was about ≈ 2 kJ/mm. The details of the welding technique used have been mentioned in Section 2.1, and are not restarted here. Figure VIII.1 shows the macrograph of the heat affected zone adjacent to the capping layer of the multirun weld (see the low magnification macrograph, Figure II.4). The austenite grain size near the fusion boundary is very large, of the order of 200μm. The corresponding detailed microstructures in different regions of Figure VIII.1 are shown in Figure VIII.2a-j. (For example, Figure VIII.2a corresponds to the region marked a and Figure VIII.2b corresponds to the region marked b in Figure VIII.1, etc.) It is apparent that in the coarse austenite grain zone, the Widmanstätten ferrite grows mainly from the allotriomorphic ferrite-austenite boundaries in the form of secondary Widmanstätten ferrite plates. The microstructure in this zone also contains large amounts of martensite, with some allotriomorphic ferrite and Widmanstätten ferrite, making the zone brittle, and susceptible to cold cracking and reheat cracking. As the austenite grain size decreases (Figure VIII.2c), the amount of allotriomorphic ferrite increases significantly simply because of the large interfacial area of austenite grain boundaries

available for allotriomorphic ferrite nucleation and growth. Figure VIII.2c illustrates the transition from the coarse austenite grain zone to a more refined structure. The micrograph also shows that when the austenite grain size is smaller than a critical value ($\approx 20\mu m$), the Widmanstätten ferrite and martensite do not form, the transformation products being just allotriomorphic ferrite and fine pearlite (the presence of fine pearlite has been established by transmission electron microscopy as shown in Figure VIII.3). The typical microstructure of the fine grained region is presented in Figure VIII.2d, consisting of allotriomorphic ferrite and fine pearlite. Figure VIII.2e clearly shows the transition from the austenite grain refined region to a partially transformed region; the peak temperature of this transition boundary is Ar_3. Some of the untransformed original pearlite in this region has been spheroidised, as illustrated in Figure VIII.2f. Figure VIII.2g displays the transition boundary (peak temperature Ar_1) from the partially transformed zone to the tempered zone. The pearlitic colonies in this tempered zone (Figure VIII.2h) are spheroidised to a lesser extent than in the partially transformed zone consistent with the lower temperature experienced. The detailed microstructure of the pearlite colonies in the tempered zone has been examined by transmission electron microscopy (Figure VIII.4). The electron micrograph shows that the lamellar cementite has been partially spheroidised. The transition boundary from the tempered zone to unaffected zone is of coarse rather diffuse and is shown in Figure VIII.2i. The cementite layers of course pearlite (Figure VIII.2j) can clearly be seen in the unaffected base material which contains about 0.75 volume fraction of ferrite and 0.25 volume fraction of pearlite.

The austenite grain size in the heat affected zone has been measured using a linear intercept method. Because austenite grains adjacent the fusion boundary are very large, only fifteen of them could be taken into account. The plot of austenite grain size versus distance from the fusion boundary is presented in Figure VIII.5. Hardness measurements were made on the polished and etched specimens, using a Vicker's micro-hardness machine. A load of 0.5 kg was used, and the indentation was large enough to cover the specific representative microstructure in the different sub-zone of the HAZ. The hardness profile in the HAZ adjacent to the capping layer of the multirun weld is shown in Figure VIII.6. It is clear that the hardness increases with austenite grain size and reaches a maximum value near the fusion boundary. The hardness of the partially transformed zone and the tempered zone are slightly higher than that of the unaffected base plate.

8.3 The Influence of Austenite Grain Size on the Kinetics of Transformation

In order to predict the microstructure of the heat affected zone, a knowledge of transformation kinetics is vital. The work presented here is limited initially to a

193

characterisation of the influence of austenite grain size on the kinetics of the allotriomorphic ferrite transformation. A theory for allotriomorphic ferrite formation proposed by Bhadeshia et al. [39] will first be reviewed in Section 8.3.1. Isothermal dilotometric experiments have also been carried out and the results will be presented in Section 8.3.2.

8.3.1 Theory for Allotriomorphic Ferrite Formation

Recently, Bhadeshia et al. [39] have presented a new model for the development of microstructure in welds, in which the allotriomorphic ferrite grains prior to site-saturation are modelled as discs(parallel to the austenite grain boundary planes of half-thickness q, radius ηq). The aspect ratio η of the allotriomorphs is considered constant because in reality, the lengthening and thickening processes are coupled. Soft impingement between allotriomorphs growing from opposite grain boundaries should not occur at the usual cooling rates encountered in welding, and this analysis takes account of hard impingement. It has been demonstrated [39] that this disc model is a better approximation than the layer model (see Figure I.4). The detailed theory for the disc model is discussed briefly as follows.

The analysis uses the concept of extended area or volume [178]. Consider a plane surface of total area O parallel to a particular boundary. The extended area O_α^e is defined as the sum of the areas of intersection of the discs with this plane. It ensues that the change dO_α^e in O_α^e due to disc nucleated between $t=\tau$ and $t=\tau+d\tau$ is:

$$dO_\alpha^e = \pi O_b I_B [(\eta \alpha_1)^2 (t - \tau)]d\tau \qquad \text{(VIII.1)}$$

$$\text{for } \alpha_1 (t-\tau)^{0.5} > y$$

$$\text{and } dO_\alpha^e = 0$$

$$\text{for } \alpha_1 (t-\tau)^{0.5} < y$$

where O_α^e = extended area due to α allotriomorph,

O_b = area of a particular grain boundary,

I_B = grain boundary nucleation rate per unit area,

η = ratio of length to thickness of allotriomorph,

α_1 = one-dimensional parabolic thickening rate constant,

τ = incubation time for the nucleation of one particle,

and y = the distance between the boundary and an arbitary plane parallel to the boundary.

It should be noted that only particles nucleated for $\tau > (y/\alpha_1)^2$ can contribute to the extended area intersected by the plane at y, the whole extended area is given by:

$$O_\alpha^e = \int_0^{t-(y/\alpha_1)^2} (\eta\alpha_1)^2 \pi O_b I_B (t-\tau) d\tau$$

$$= 0.5\pi O_b I_B (\eta\alpha_1)^2 t^2 [1 - \theta^4] \tag{VIII.2}$$

where $\theta = y/\alpha_1 t^{0.5}$

The relationship between extended area O_α^e and and actual area O_α is given by [178]

$$O_\alpha^e \, / \, O = -\ln\{1 - [O_\alpha \, / \, O]\}$$

Therefore $O_\alpha = O_b(1- \exp\{-O_\alpha^e/O_b\})$ \hfill (VIII.3)

Assuming that there is no interference with allotriomophs from other boundaries, the total volume V_b of material originating from this grain boundary is given by integrating for all y between negative and positive infinity; in terms of θ, the integral amounts to:

$$V_b = \int_0^1 2(\alpha_1 t^{0.5}) O_b (1- \exp\{-O_\alpha^e/O_b\}) d\theta$$

$$= \int_0^1 2 O_b (\alpha_1 t^{0.5})(1- \exp\{-0.5\pi I_B (\eta\alpha_1)^2 t^2 [1-\theta^4]\}) d\theta$$

$$= 2 O_b (\alpha_1 t^{0.5}) f\{\theta, \eta\alpha_1, I_B, t\} \tag{VIII.4}$$

where $f\{\theta, \eta\alpha_1, I_B, t\} = \int_0^1 (1- \exp\{-0.5\pi I_B (\eta\alpha_1)^2 t^2 [1-\theta^4]\}) d\theta$

If the total grain boundary area is $O_B = \Sigma O_B$, then by substituting O_B for O_b in equation VIII.4 the total extended volume V_α^e of material emanating from all boundaries is found; this is an extended volume because allowance was not made for impingement of discs originating from different boundaries. Therefore,

$$V_\alpha^e = 2 O_B (\alpha_1 t^{0.5}) f\{\theta, \eta\alpha_1, I_B, t\}$$

and if V is the total volume, and S_v the austenite grain surface area per unit volume, then:

$$V_\alpha^e \, / \, V = 2 S_v (\alpha_1 t^{0.5}) f\{\theta, \eta\alpha_1, I_B, t\}$$

195

It can be converted into the actual volume, V_α, using the equation:

$$V_\alpha \, / \, (V\phi) = 1 - \exp\{-V_\alpha^e \, / \, (V\phi)\}$$

$$\text{where } \phi = (x^{\gamma\alpha} - \bar{x})/(x^{\gamma\alpha} - x^{\alpha\gamma})$$

Finally, it follows that:

$$-\ln\{1 - \zeta\} = (2S_v/\phi)(\alpha_i t^{0.5})f\{\theta, \eta\alpha_i, I_B, t\} \qquad \text{(VIII.5)}$$

where ζ the volume of α divided by its equilibrium volume, i.e.,

$$\zeta = V_\alpha \, / \, (V\phi) \, .$$

As I_B increases or time increases, the value of the integral f tends to unity due to site saturation. In this condition, equation VIII.5 simplifies to one dimensional thickening:

$$- \ln\{1-\zeta\} = (2S_v \, / \, \phi)(\alpha_i t^{0.5}) \qquad \text{(VIII.6)}$$

The relationship between $\bar{L}$ the mean linear intercept for austenite grains and S_v the austenite grain surface area per unit volume, can be written as:

$$S_v = 2 \, / \, \bar{L} \, .$$

It is clear that equation VIII.5 already provides an interpretation of austenite grain size effect on the kinetics of allotriomorphic ferrite transformation. However, theory is still needed for the prediction of ferrite nucleation rates.

8.3.2 Dilatometry

This work studied here is initially limited to isothermal dilatometry, and the austenite grain size effect on the kinetics of allotriomorphic ferrite transformation has been investigated. The experimental technique is essentially the same as in Section 3.2. The experiments were carried out on the homogenised base materials austenitised at four different temperature 870, 950, 1100 and 1200°C, respectively, for 10 minutes, and then isothermally transformed in a temperature range (680~760°C) for only allotriomorphic ferrite reaction. The austenite grain sizes have been measured using linear intercept method on the optical specimens, and are 16±3, 25±5, 46±8, 159±22μm, respectively, for the specimens austenitised at 870, 950, 1100 and 1200°C for 10 minutes. The isothermal

196

dilatometric curves for allotriomorphic ferrite formation are shown in Figure VIII.7(a)~(e).

Figure VIII.7(a) shows isothermal transformation of allotriomorphic ferrite at 760°C for the four different starting austenite grain sizes. The amount of the transformation is very small even for a very long time in any one of the four cases, and this implies that 760°C is very close to the Ae_3 temperature. It also clearly demonstrates that the time taken for the initiation of allotriomorphic ferrite transformation becomes significantly longer as the austenite grain size increases. Figure VIII.7(b)~(e) present the same tendency in grain size effect; i.e., when austenite grain size is small, the transformation rate of allotriomorphic ferrite will be large. For the same grain size of austenite, the transformation rate increases as the isothermal transformation temperature decreases from 760°C to 680°C. Figure VIII.7(e) shows that at isothermal temperature 680°C the incubation time of allotriomorphic ferrite transformation is too small to detect for the austenite grain sizes 16 and 25μm (austenitised at 870°C and 950°C, respectively, for 10 minutes). This indicates that the nose of diffusional C curve is in the vicinity of 680°C. All the dilatometric data consistently show that as the austenite grain size decreases, the amount of allotriomorphic ferrite transformation increases at the same isothermal temperature for the same period of time. This indicates that the grain boundary area is a important factor in the kinetics of transformation of allotriomorphic ferrite.

The microstructure of dilatometer specimens has also been studied (Figure VIII.8). The optical micrograph (Figure VIII.8a) shows a few allotriomorphs forming after austenitisation of base metal at 1200°C for 10 minutes followed by isothermal transformation at 760°C for 2 hours prior to quenching to ambient temperature (the helium gas quenching rate in dilatometer ≈60°C/s). Because of kinetic restrictions (large austenite grain size), the residual austenite has mainly transformed to martensite, some bainite and a small amount of Widmanstätten ferrite. On the other hand, Figure VIII.8b shows the microstructure for the dilatometric specimen austenitised at 870°C for 10 minutes followed by isothermal transformation at the same 760°C for 2 hours before quenching to room temperature. It is clear that a large amount of allotriomorphic ferrite forms during cooling in this case. (Dilatometric curves in Figure VIII.7a shows little transformation at 760°C for 2 hours). The optical micrographs (Figures VIII.8c and d) show the microstructure for the specimens austenitised at 1200°C and 1100°C, respectively, for 10 minutes followed by isothermal transformation at 720°C for 2 hours before quenching to room temperature. The results show that the austenite grain boundaries rapidly become decorated with a layer of polycrystalline allotriomorphic ferrite, and besides the allotriomorphic ferrite the microstructure consists chiefly of martensite, with some bainite and Widmanstätten ferrite. Comparing the microstructure shown in Figure VIII.8c and that in Figure VIII.8d, it is found that the latter (small

197

austenite grain size) contains a higher volume fraction of Widmanstätten ferrite. It should be noted that as the isothermal transformation temperature is reduced (for example at 700 and 680°C), the carbon composition of residual austenite will increase due to the partitioning of carbon between α and γ, and the transformation during cooling will be influenced. Figures VIII.8e and f present the corresponding microstructure for the specimens austenitised at 1200°C and 1100°C, respectively, for 10 minutes followed by isothermal transformation at 700°C for 2 hours before quenching to room temperature. Figures VIII.8g and h show the corresponding microstructure for the specimens austenitised at 1200°C and at 1100°C, respectively, for 10 minutes followed by isothermal transformation at 680°C for 2 hours before quenching to ambient temperature. It is clear that when the carbon content of the residual austenite is large, the formation of Widmanstätten ferrite during quenching is suppressed.

8.3.3 Further Study

It is necessary to convert the dilatometric data (Figure VIII.7) from "the relative length change versus time" to "the volume fraction of allotriomorphic ferrite formed versus time", for the purpose of investigating quantitatively kinetics of allotriomorphic ferrite transformation. The calculation is the same as given by equation III.1, and the linear expansion coefficients and lattice parameters of ferrite and austenite are required. It will be interesting to compare experimental data with the model discussed in Section 8.3.1.

Equation VIII.6 can be written as:

$$V_\alpha/V = \phi \, [1-\exp\{-(2S_v/\phi)(\alpha_1 t^{0.5})\}]$$

(VIII.7)

Therefore, after determining S_v and α_1 value, the theoretical data can be calculated. This forms a basis for future work.

8.4 Summary

The microstructure of the heat affected zone adjacent to the capping layer of a multirun weld has been studied. It has been found that as austenite grain decreases, the rate of allotriomorphic ferrite formation increases significantly. This is simply because of the large interfacial area of austenite grain boundaries available for allotriomorphic ferrite nucleation and growth. A theory which provides an interpretation of austenite grain size effect on the kinetics of allotriomorphic ferrite transformation has been reviewed. The isothermal dilatometric experiments have also been carried out, and the kinetic data has been obtained. It needs more work to elucidate the kinetic theory.
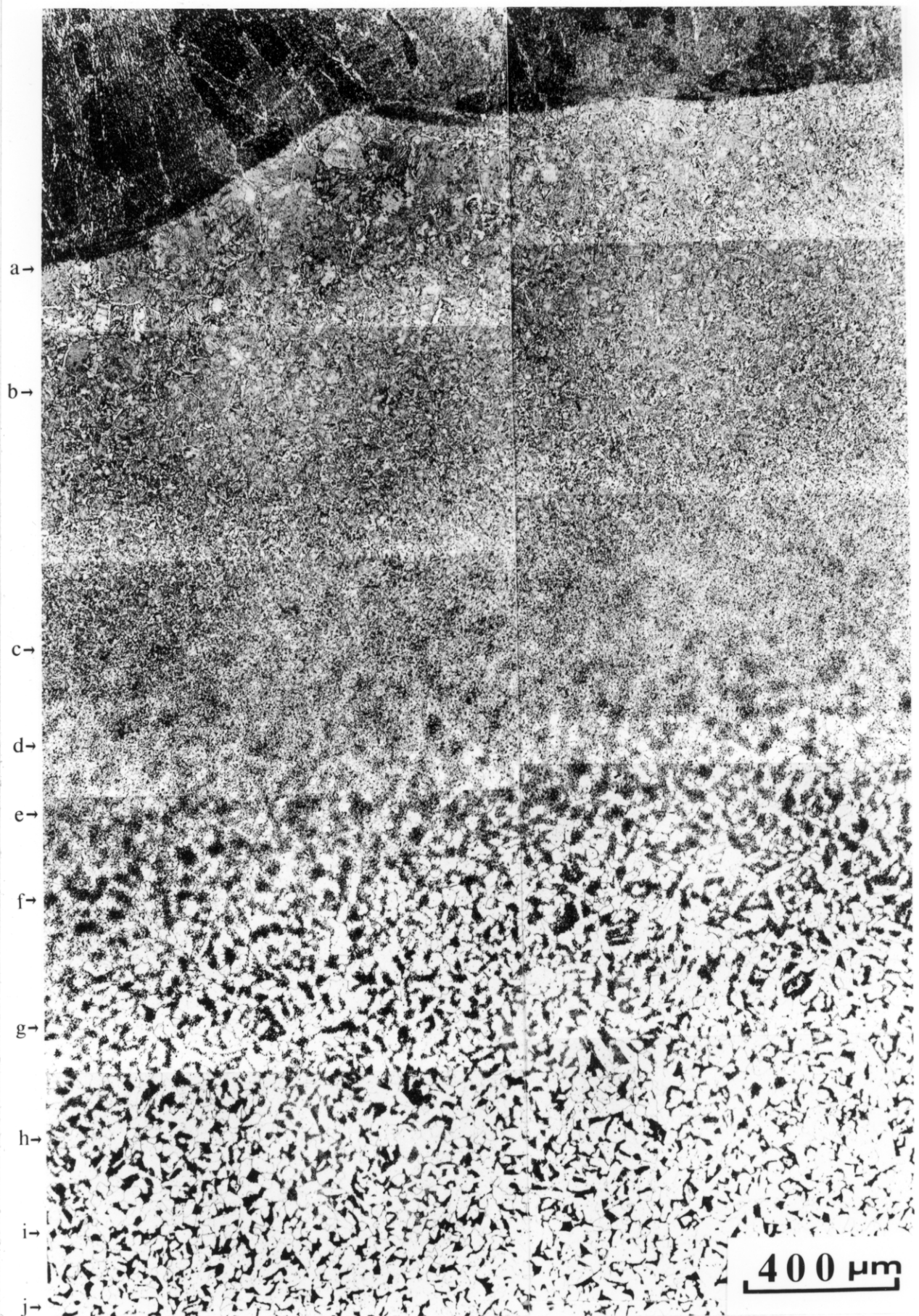
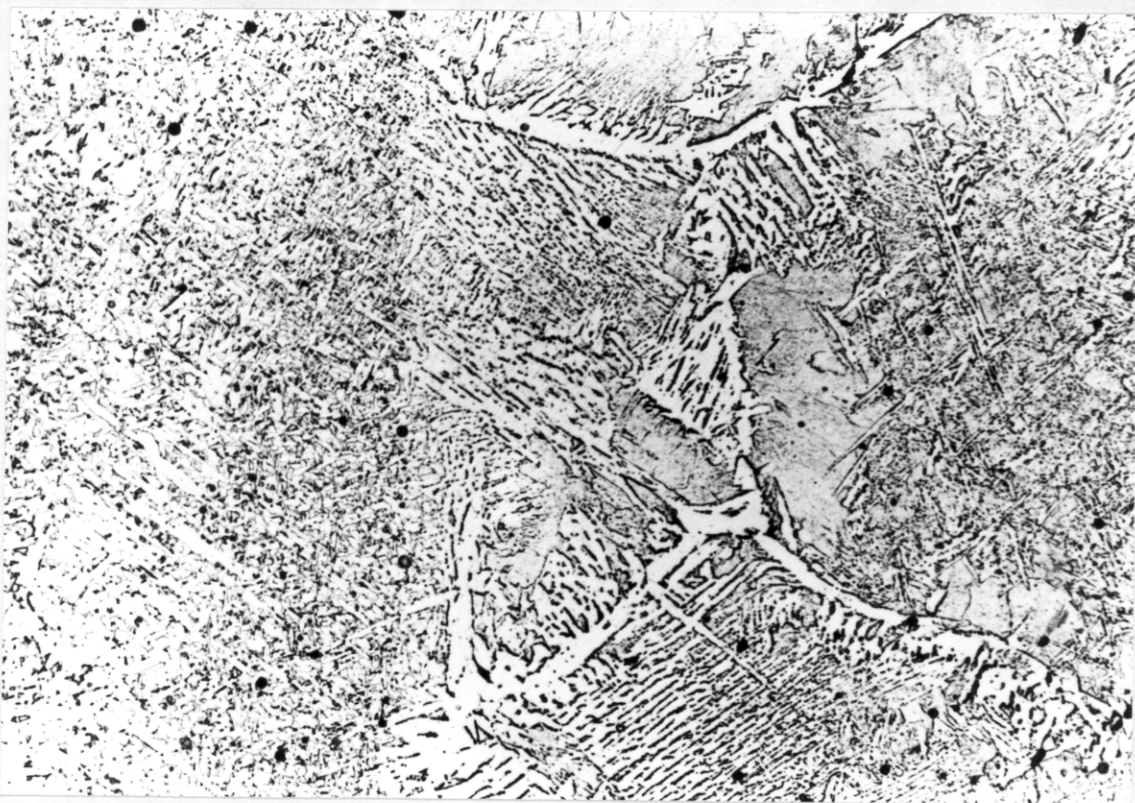Figure VIII.1 - Showing the macrograph of heat affected zone adjacent to the capping layer of the multirun weld.

Figure VIII.2a - Microstructure corresponds to the region marked a in Figure VIII.1. The micrograph shows the microstructure adjacent to the fusion boundary. The microstructure of HAZ in this region contains some allotriomorphic ferrite and Widmanstätten ferrite and large amount of martensite (grey areas).   └20µm┘
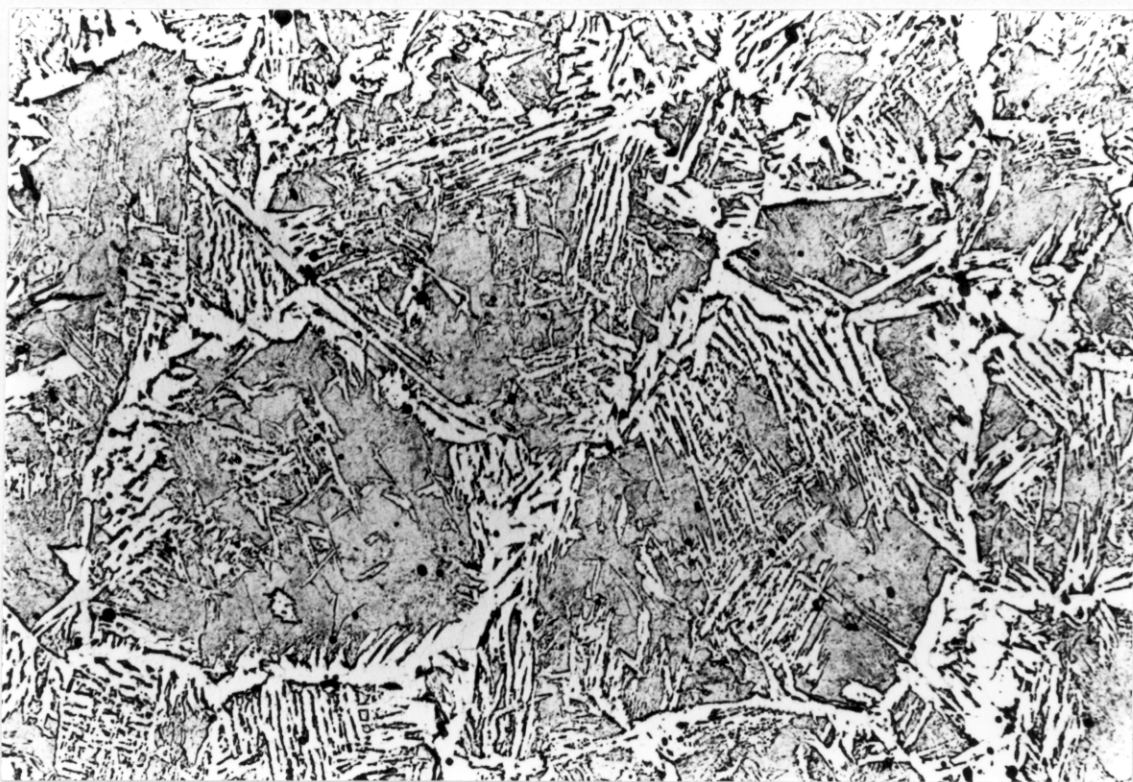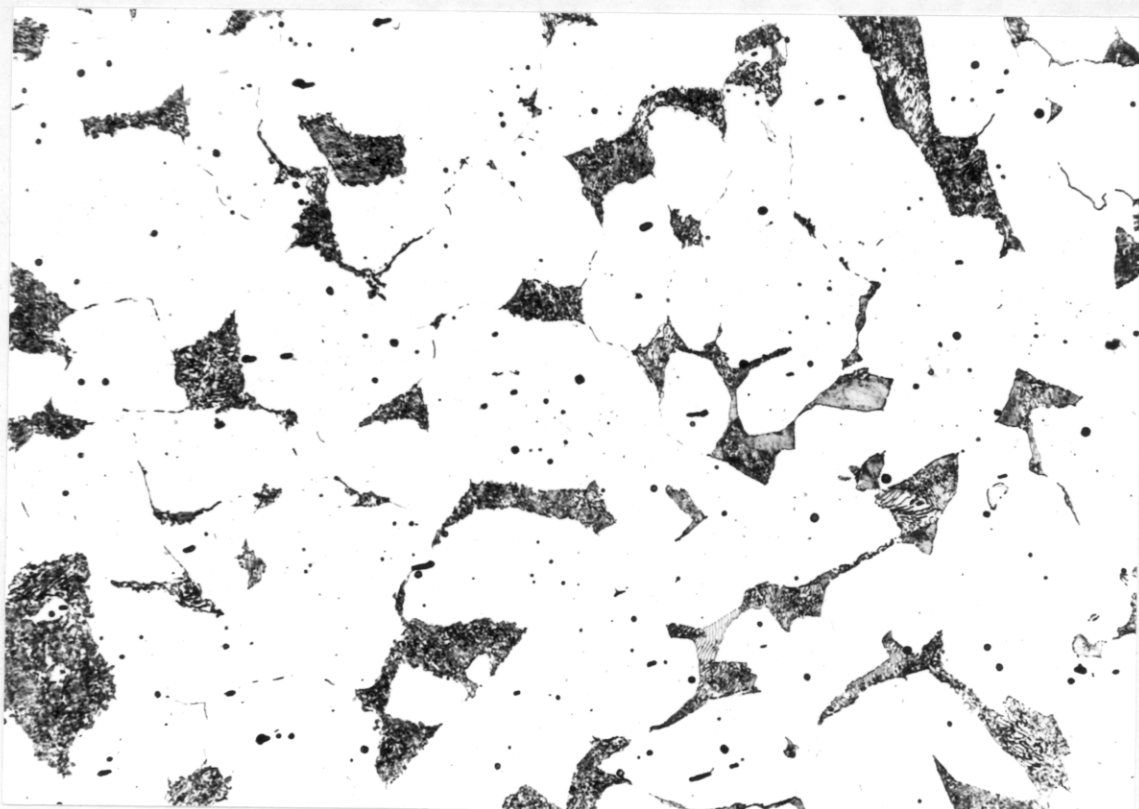

Figure VIII.2b - Microstructure corresponds to the region marked b in Figure VIII.1.
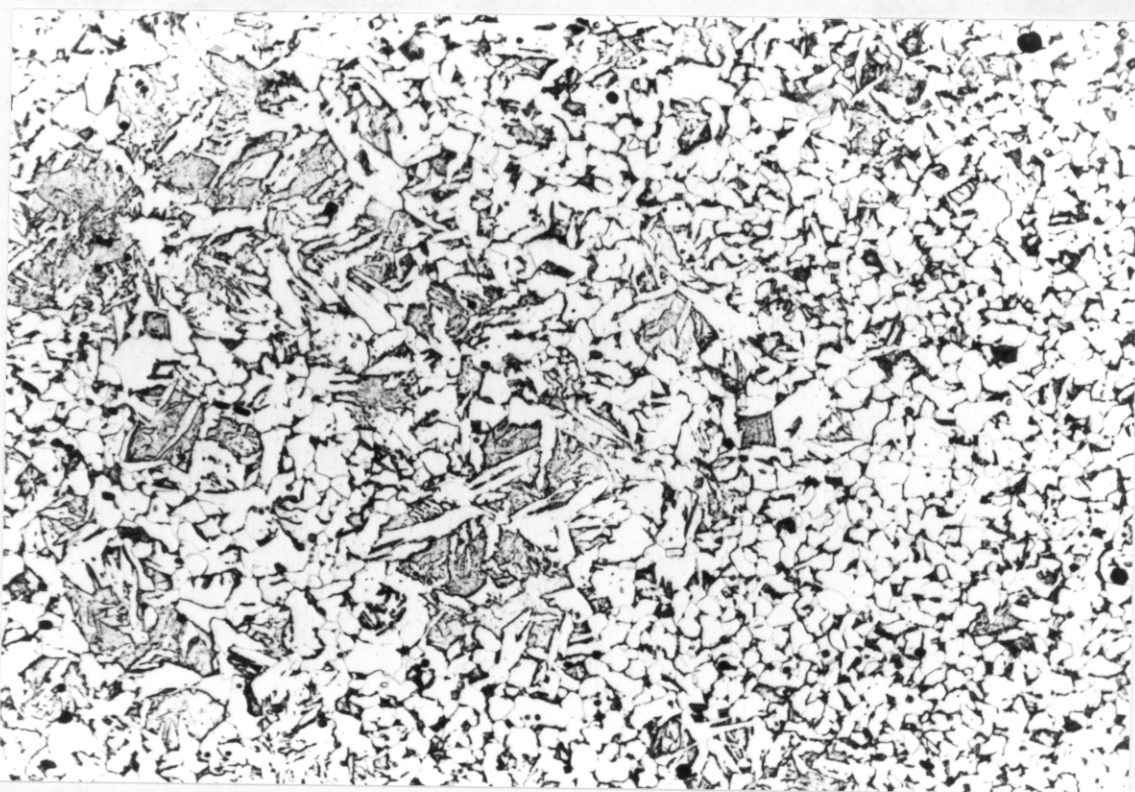
Figure VIII.2c - Microstructure corresponds to the region marked c in Figure VIII.1. 20μm
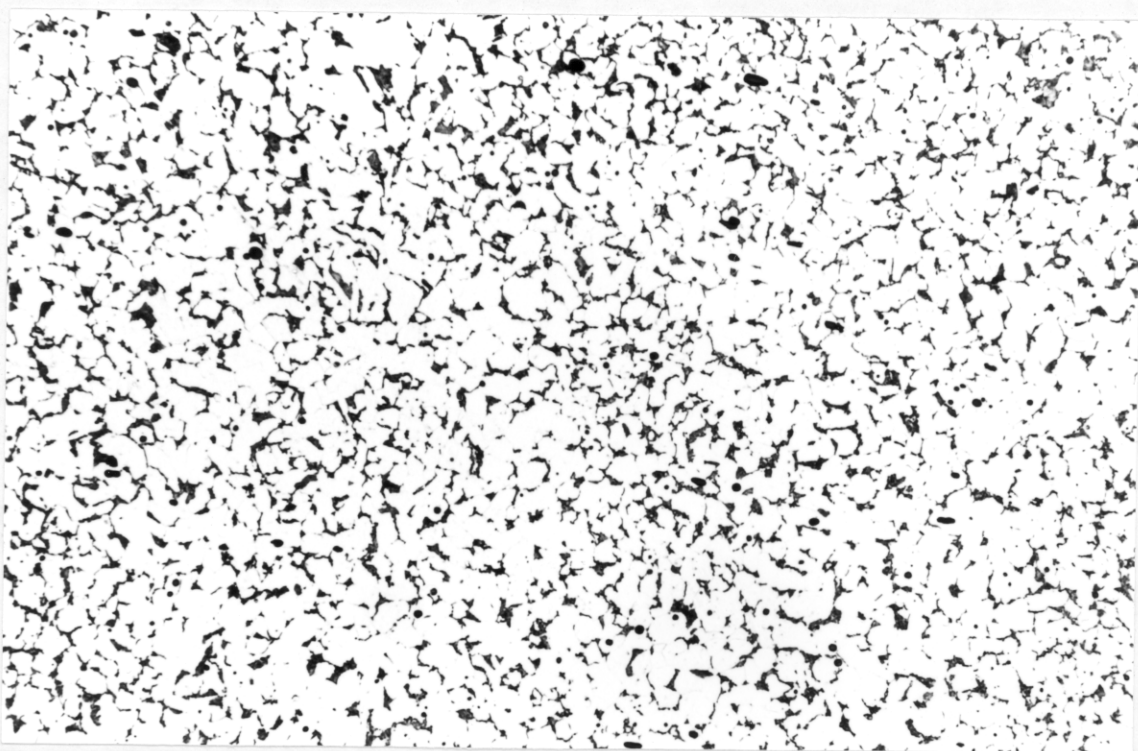
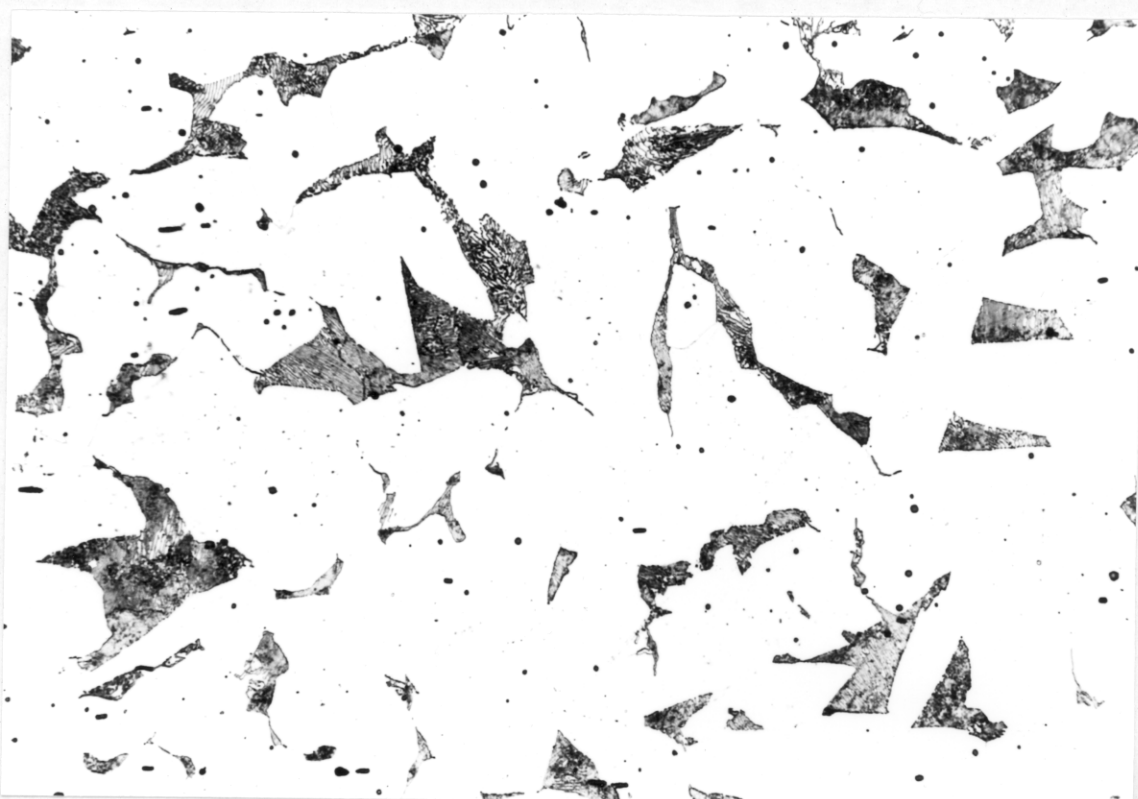Figure VIII.2d - Microstructure corresponds to the region marked d in Figure VIII.1. 20μm
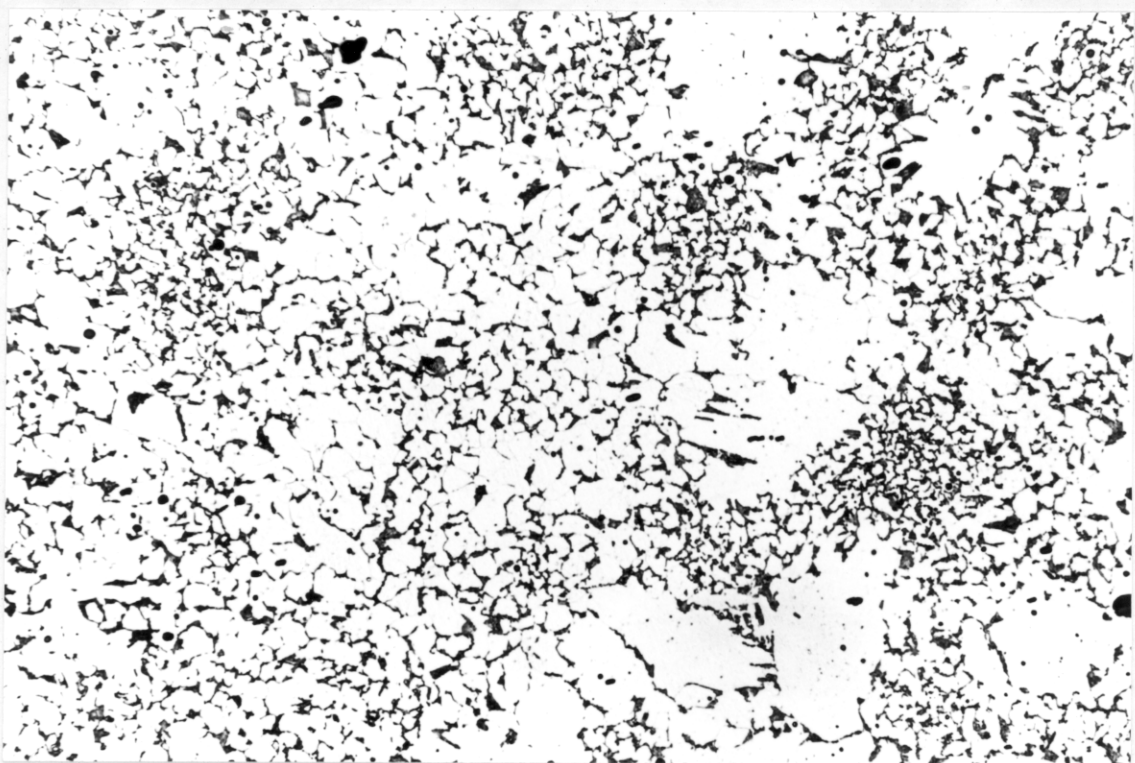
Figure VIII.2e - Microstructure corresponds to the region marked e in Figure VIII.1. 20μm
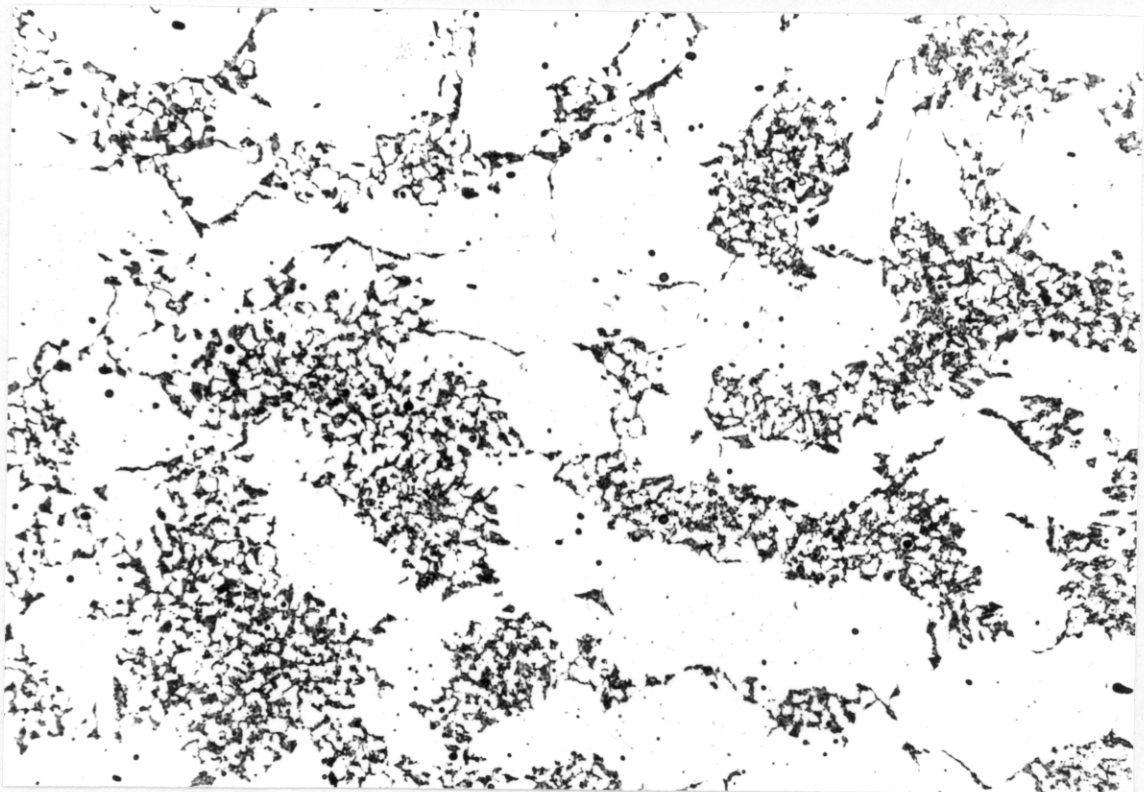
Figure VIII.2f - Microstructure corresponds to the region marked f in Figure VIII.1. 20μm
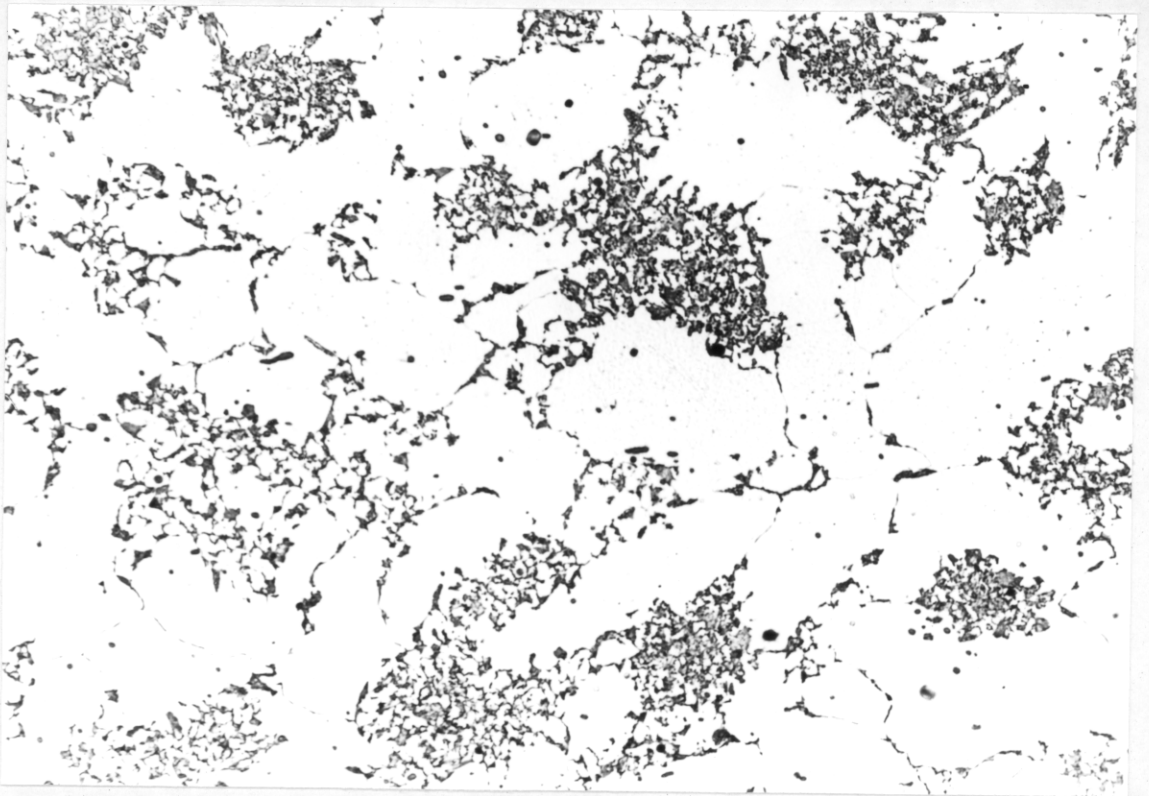
Figure VIII.2g - Microstructure corresponds to the region marked g in Figure VIII.1. 20 µm
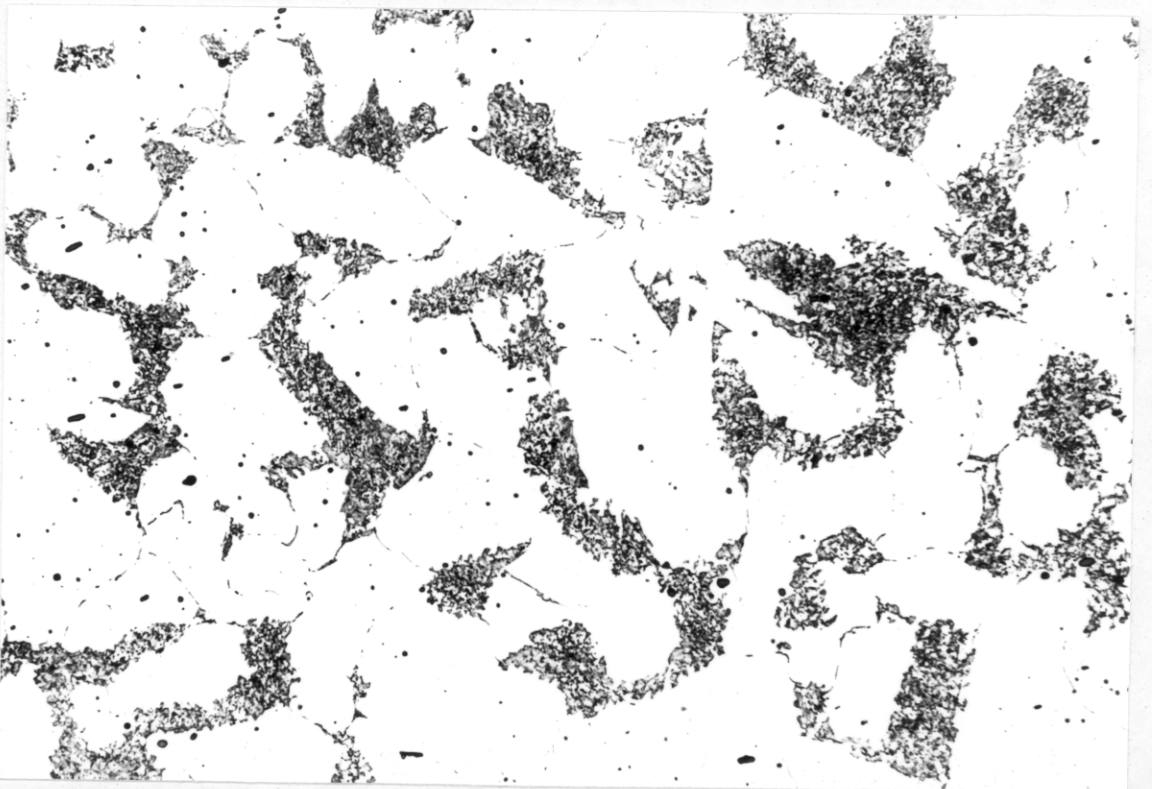
Figure VIII.2h - Microstructure corresponds to the region marked h in Figure VIII.1. 20 µm

Figure VIII.2i - Microstructure corresponds to the region marked i in Figure VIII.1. 20 μm

Figure VIII.2j - Microstructure corresponds to the region marked j in Figure VIII.1. 20 μm
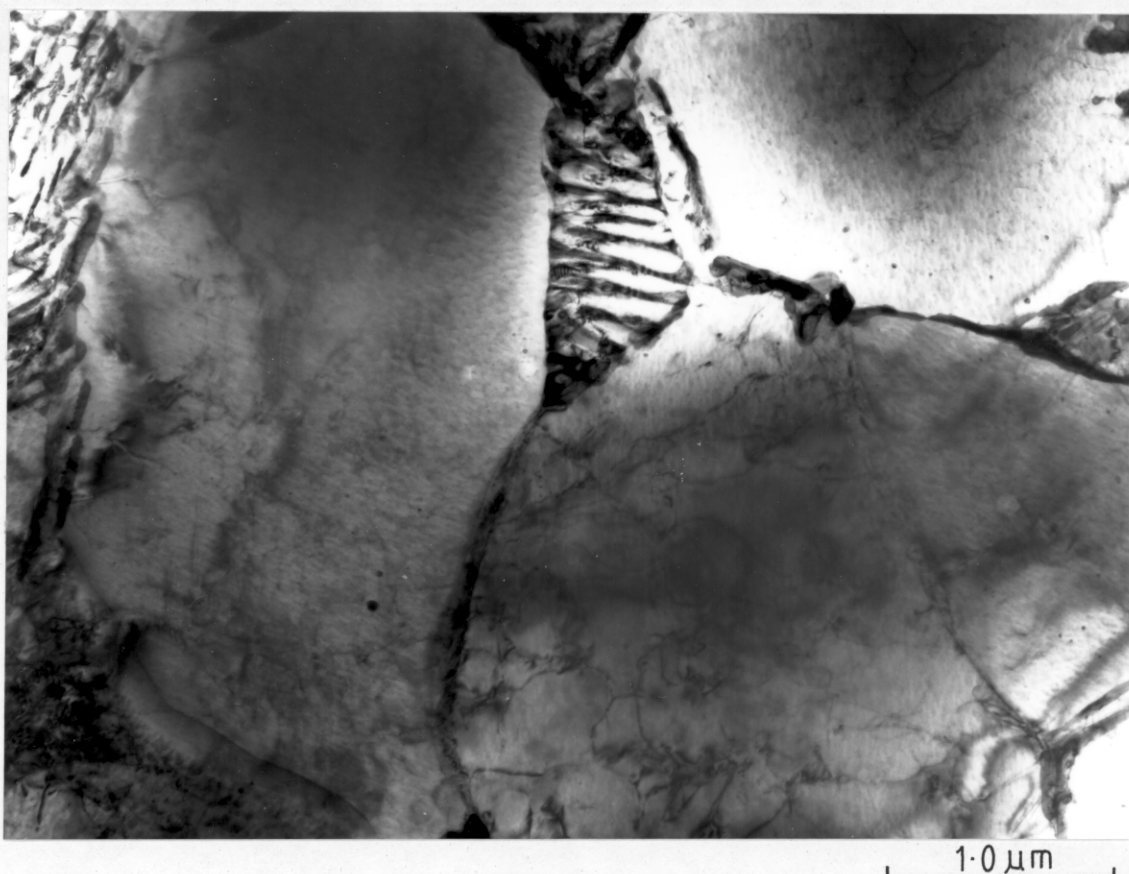
Figure VIII.3 - Electron micrograph shows fine pearlite in the austenite grain refined zone.
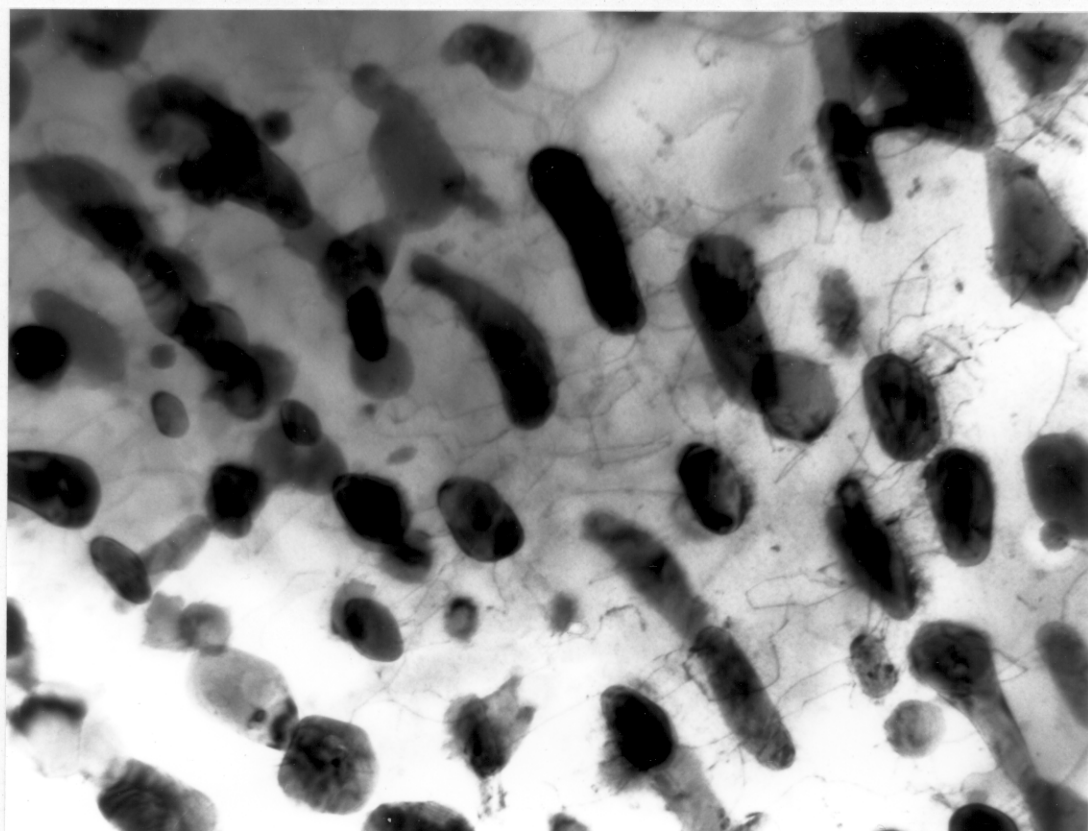
Figure VIII.4 - Electron micrograph shows that the lamellar cementite has been partially spheroidised.
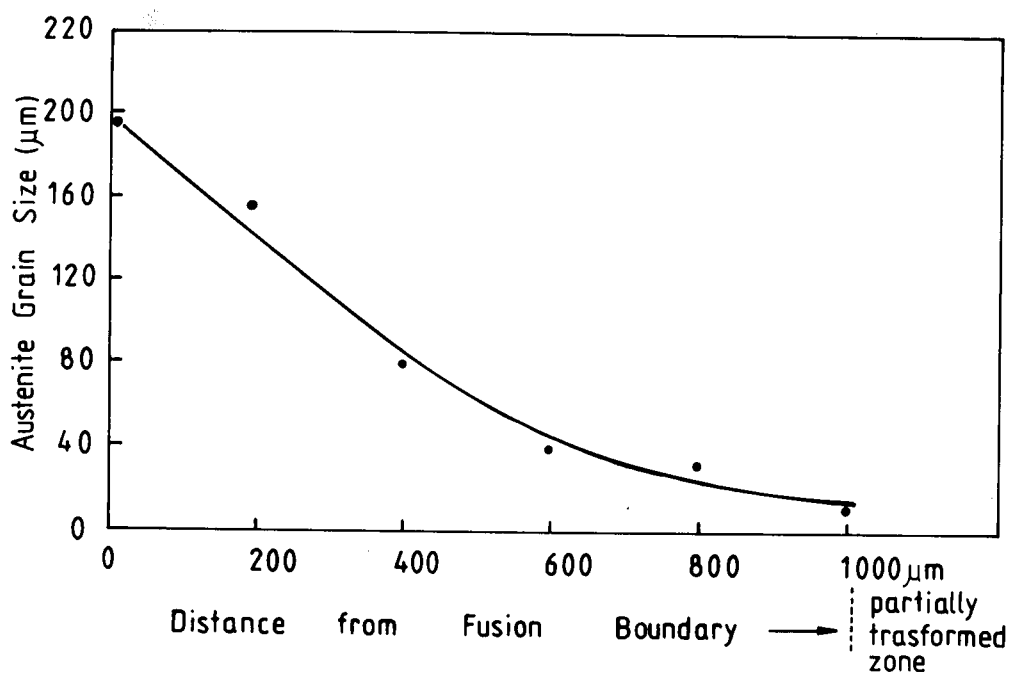
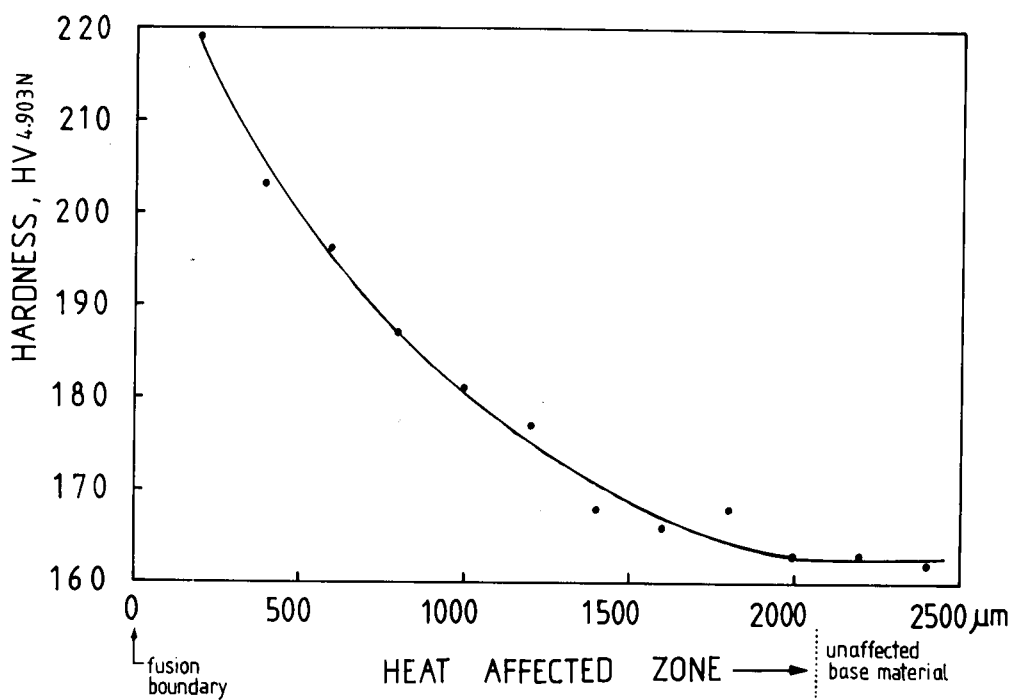Figure VIII.5 - Showing the austenite grain size versus the distance from the fusion boundary.

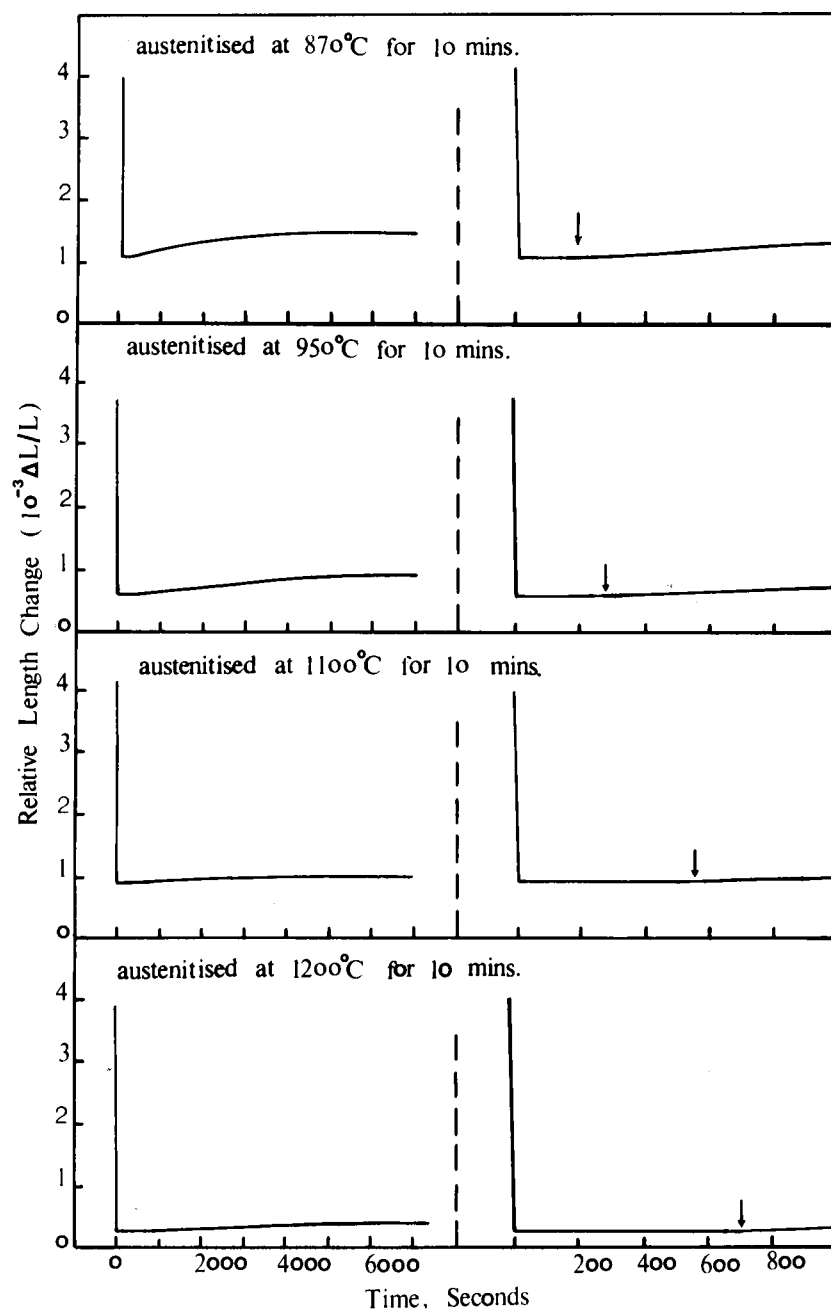Figure VIII.6 - Showing the hardness profile in heat affected zone.

Figure VIII.7(a) - Dilatometric curves show isothermal transformation at 760°C. The left part of the figure presents for the long isothermal transformation time; the right part, for the short isothermal transformation time.
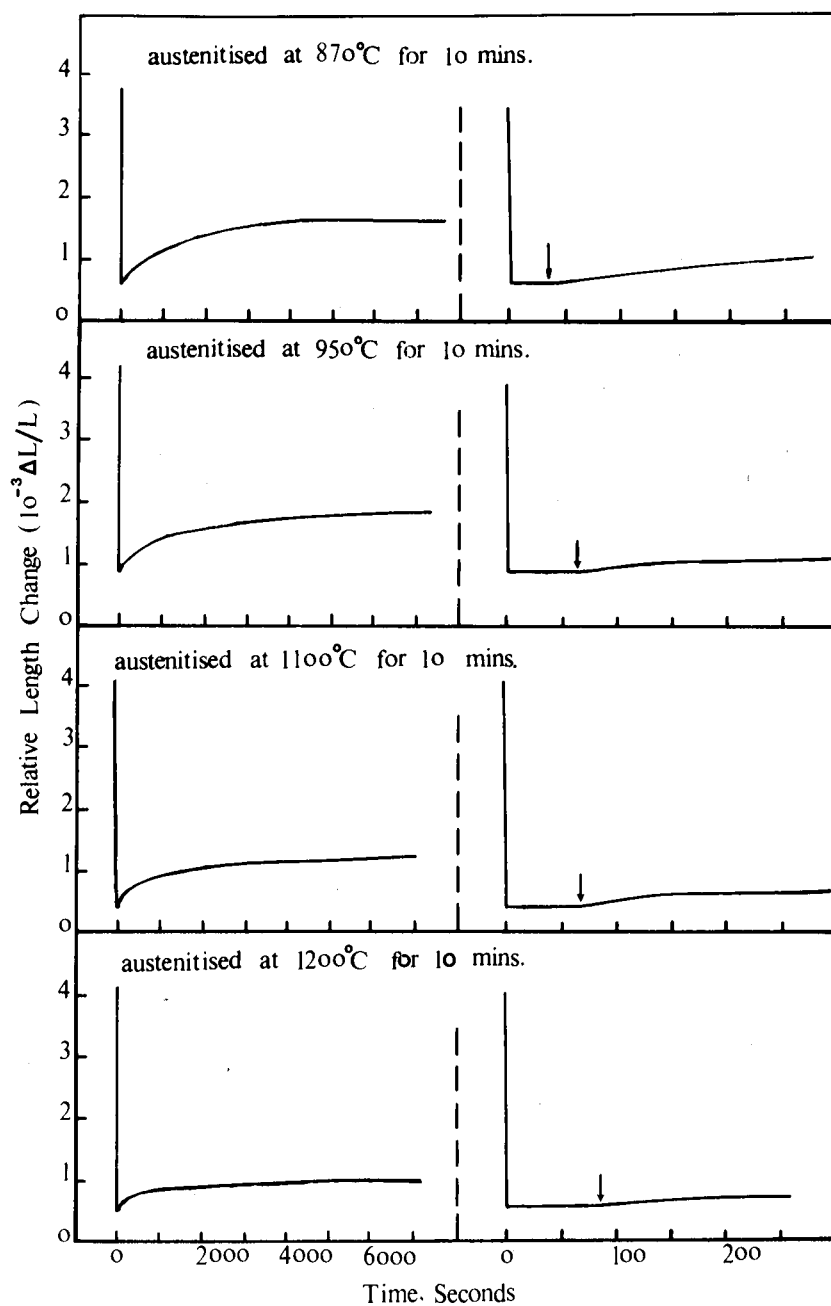
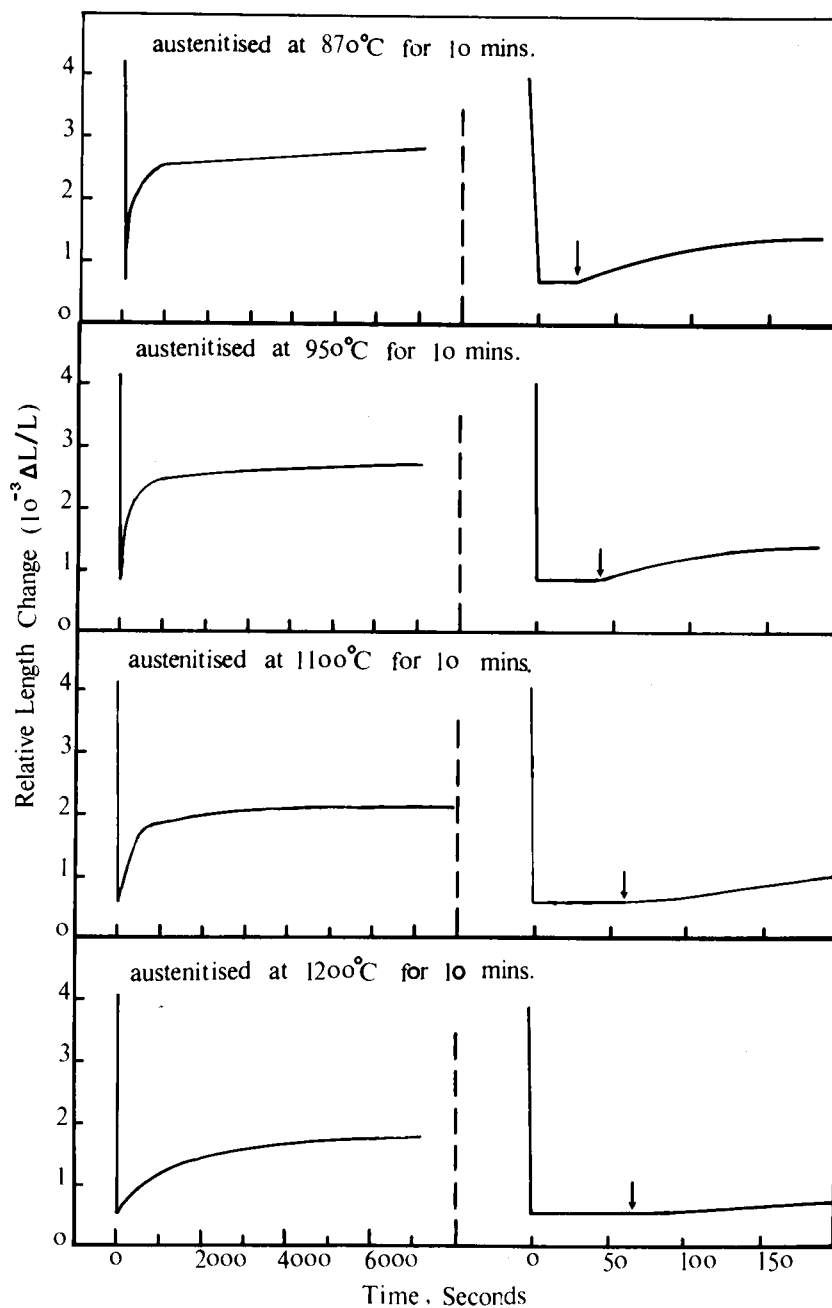Figure VIII.7(b) - Dilatometric curves show isothermal transformation at 740°C.

208

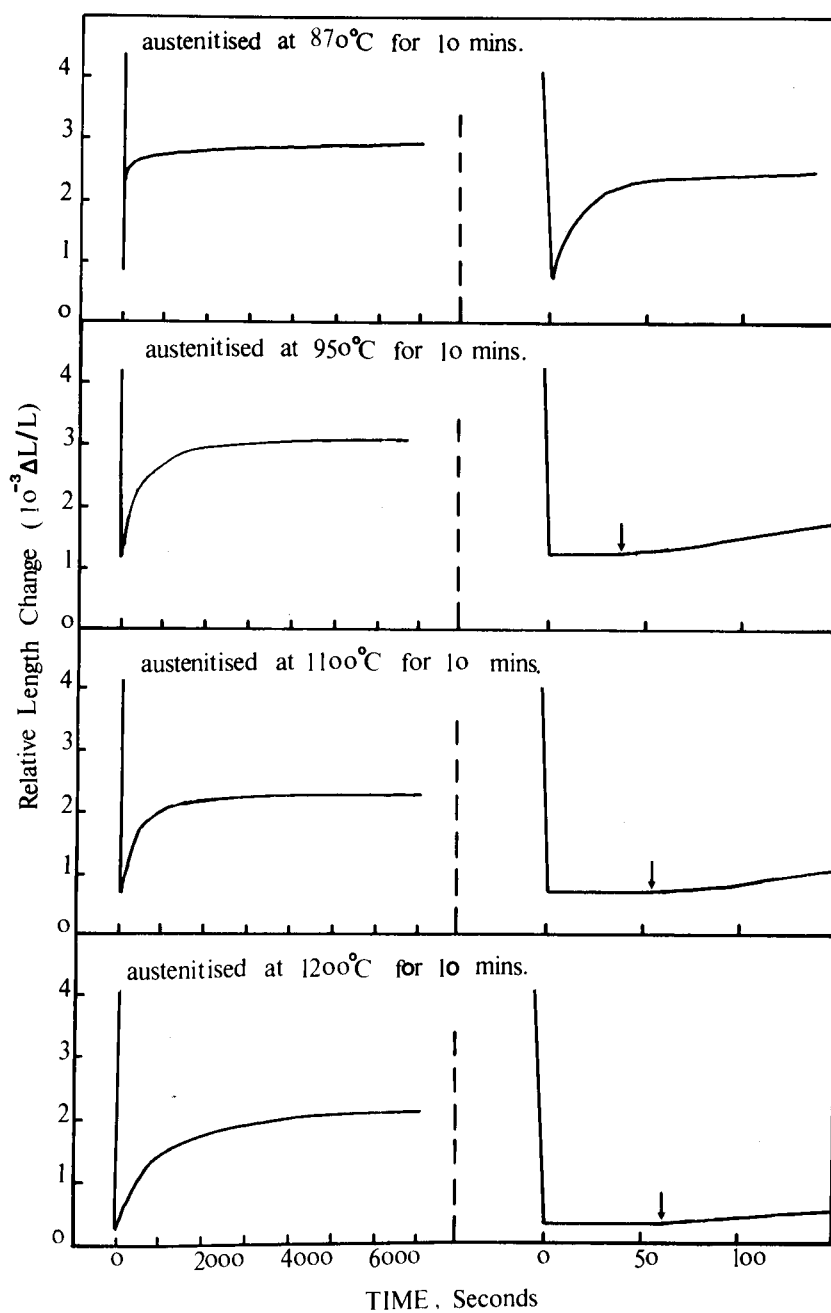Figure VIII.7(c) - Dilatometric curves show isothermal transformation at 720°C.

Figure VIII.7(d) - Dilatometric curves shows isothermal transformation at 700°C.